Fluids and Barriers of the CNS

RESEARCH

Open Access

A patient-derived amyotrophic lateral sclerosis blood-brain barrier model for focused ultrasound-mediated anti-TDP-43 antibody delivery

Joanna M. Wasielewska[1,2], Juliana C. S. Chaves[1], Mauricio Castro Cabral-da-Silva[3,4], Martina Pecoraro[5], Stephani J. Viljoen[1,8], Tam Hong Nguyen[6], Vincenzo La Bella[5], Lotta E. Oikari[1,7], Lezanne Ooi[3] and Anthony R. White[1,7,8,9*]

Abstract

Background Amyotrophic lateral sclerosis (ALS) is a rapidly progressing neurodegenerative disorder with minimally effective treatment options. An important hurdle in ALS drug development is the non-invasive therapeutic access to the motor cortex currently limited by the presence of the blood-brain barrier (BBB). Focused ultrasound and microbubble (FUS^{+MB}) treatment is an emerging technology that was successfully used in ALS patients to temporarily open the cortical BBB. However, FUS^{+MB}-mediated drug delivery across ALS patients' BBB has not yet been reported. Similarly, the effects of FUS^{+MB} on human ALS BBB cells remain unexplored.

Methods Here we established the first FUS^{+MB}-compatible, fully-human ALS patient-cell-derived BBB model based on induced brain endothelial-like cells (iBECs) to study anti-TDP-43 antibody delivery and FUS^{+MB} bioeffects in vitro.

Results Generated ALS iBECs recapitulated disease-specific hallmarks of BBB pathology, including reduced BBB integrity and permeability, and TDP-43 proteinopathy. The results also identified differences between sporadic ALS and familial (*C9orf72* expansion carrying) ALS iBECs reflecting patient heterogeneity associated with disease subgroups. Studies in these models revealed successful ALS iBEC monolayer opening in vitro with no adverse cellular effects of FUS^{+MB} as reflected by lactate dehydrogenase (LDH) release viability assay and the lack of visible monolayer damage or morphology change in FUS^{+MB} treated cells. This was accompanied by the molecular bioeffects of FUS^{+MB} in ALS iBECs including changes in expression of tight and adherens junction markers, and drug transporter and inflammatory mediators, with sporadic and C9orf72 ALS iBECs generating transient specific responses. Additionally, we demonstrated an effective increase in the delivery of anti-TDP-43 antibody with FUS^{+MB} in C9orf72 (2.7-fold) and sporadic (1.9-fold) ALS iBECs providing the first proof-of-concept evidence that FUS^{+MB} can be used to enhance the permeability of large molecule therapeutics across the BBB in a human ALS in vitro model.

*Correspondence:
Anthony R. White
tony.white@qimrberghofer.edu.au

Full list of author information is available at the end of the article

Conclusions Together, this study describes the first characterisation of cellular and molecular responses of ALS iBECs to FUS^{+MB} and provides a fully-human platform for FUS^{+MB}-mediated drug delivery screening on an ALS BBB in vitro model.

Keywords Amyotrophic lateral sclerosis, Blood-brain barrier, In vitro model, Antibody, TDP-43, Drug delivery, Focused ultrasound

Background

Amyotrophic lateral sclerosis (ALS) is a neurodegenerative disorder characterised by the gradual loss of motor neurons [1]. Despite major progress in ALS drug discovery, the effective translation of preclinical therapeutic agents to their clinical application in ALS patients remains limited, with approved therapeutics offering only a modest increase in life expectancy [1, 2].

ALS pathophysiology is complex, with multiple interacting pathways involving genetic mutations, neuroinflammation, neurotransmitter excitotoxicity, oxidative stress and proteinopathy converging into upper and lower motor neuron degeneration [1]. Correspondingly, extensive evidence suggests early pathological changes in the upper motor neurons in the motor cortex supporting the development of motor cortex-directed therapies [3–9]. However, targeting cortical neurons provides challenges due to the presence of the blood-brain barrier (BBB), which markedly limits the penetration of ALS therapeutics into the central nervous system (CNS) [2, 10–14].

Additionally, evidence from animal and human studies indicates BBB dysfunction in ALS and suggests cerebrovascular involvement in disease development and progression [15–18]. Changes in BBB ultrastructure and barrier integrity were found in preclinical models and in patients, leading to increased BBB permeability and infiltration of blood-derived proteins, erythrocytes and immune cells into the brain [16, 17, 19–24]. Others reported degeneration of BBB-forming cells including brain endothelial cells (BECs), pericytes and astrocytes, and found impaired expression of tight and adherens junctions in BECs [19, 13, 25]. In addition, alterations in expression, function and cellular distribution of BBB drug transporters such as P-glycoprotein (P-gp) and breast cancer resistance protein (BCRP) were identified in ALS [13, 26]. Collectively, these changes further contribute to the complex interaction of drugs with pathologically altered BBB limiting their clinical effectiveness. Thus, non-invasive therapeutic access to the motor cortex still poses a critical challenge in ALS drug development.

Focused ultrasound combined with activated microbubbles (FUS^{+MB}) is an innovative method facilitating temporary BBB opening, therefore enabling targeted CNS drug delivery [27]. In animal studies, the application of FUS^{+MB} aided in the delivery of ALS therapeutics across the BBB [28–30], providing additional therapeutic benefits as compared to the drug alone [29, 30]. In the first-in-human clinical study, FUS^{+MB} induced a transient increase in the leakage of contrast agent across the BBB in the motor cortex of four patients demonstrating the safety and feasibility of BBB opening in ALS [31]. However, FUS^{+MB}-mediated ALS drug delivery has not yet been achieved in humans. Similarly, the molecular effects of FUS^{+MB} on human ALS BBB cells are currently unknown.

A novel ALS patient-cell-derived in vitro platform was developed to study the bioeffects of FUS^{+MB} on human BECs and investigated FUS^{+MB}-enhanced antibody transport across ALS BBB in vitro. To accurately model the heterogeneity of the ALS BBB pathology [16] human induced pluripotent stem cells (iPSCs) from a sporadic ALS patient were used, together with cells from an individual carrying the intronic *C9orf72* hexanucleotide expansion (>30 GGGGCC) that is found in an estimated 40% of familial ALS cases [32], and differentiated them towards brain endothelial-like cells (iBECs). Results demonstrated phenotypical differences in ALS iPSC-derived iBECs as compared to healthy donor controls, as well as between sporadic and familial ALS cells, replicating some of the key features of ALS BBB pathology found in humans [24, 25]. Also presented was a lack of adverse effects of FUS^{+MB} on ALS iBECs viability and the reversibility of barrier opening in vitro, lending further support to the clinical safety of FUS^{+MB} in ALS patients. Finally, the research achieved improved delivery of anti-TDP-43 antibody with FUS^{+MB} demonstrating the applicability of FUS^{+MB} to enhance large molecule therapeutic permeability in human ALS BBB in vitro.

Together this proof-of-concept study provides the first ALS patient-cell-derived BBB model for FUS^{+MB}-enhanced therapeutic permeability screening, thereby contributing to the translational advancement of ultrasound-based therapies in ALS.

Materials and methods

Human iPSCs generation and characterisation

Three human iPSC lines were utilised in this study (Table S1). The healthy donor (HD) control line HDFa was previously generated by prof. Jose M. Polo laboratory (Monash University) and characterised by us [33, 34]. Two ALS iPSC lines were generated from patients' skin fibroblasts. A punch biopsy was obtained from the left arm of two patients clinically diagnosed with either sporadic or familial (*C9orf72*; > 30 GGGGCC repeats) ALS

(Table S2) after informed consent. The obtained biopsy was immediately placed in cold phosphate-buffered saline (PBS). The skin explant was then cut into pieces, which were cultured in Dulbecco's modified Eagle's medium supplemented with 10% calf serum, 2 mM L-glutamine, 5 mM pyruvate, 100 U/mL penicillin and 100 µg/mL streptomycin. Fibroblasts were maintained in culture and then frozen in liquid nitrogen. The respective ALS iPSC lines IT_002–04 and IT_004–04 were generated from the patient's fibroblasts using repeated mRNA transfection for pluripotency transcription factors OCT4, KLF4, SOX2, c-MYC, LIN28 and NANOG as described previously [35]. The STR profiling was performed and confirmed 100% match to the donor fibroblasts.

iPSCs from all lines were cultured in StemFlex™ medium on human recombinant vitronectin (Thermo Fisher Scientific) as described [33, 34, 36]. All iPSC lines were characterised for nuclear expression of stemness markers Nanog and SOX2 by immunofluorescence as previously described [33, 34].

Differentiation and characterisation of human induced brain endothelial-like cells (iBECs)

Induced brain endothelial-like cells (iBECs) were generated from human iPSCs as previously described [33, 34, 36, 37]. Briefly, iPSCs were plated at 20,000 cells/cm^2 on human embryonic stem cell (hESC)-qualified Matrigel (Corning) coating in StemFlex™ medium supplemented with 10 µM Rho-associated kinase inhibitor (iROCK) to initiate differentiation [33, 34, 36]. Cells were then cultured for six days in an unconditioned medium consisting of DMEM/F12+GlutaMAX (Life Technologies), 20% KnockOUT serum replacement (Life Technologies), 1 x non-essential amino acids (Life Technologies) and 0.1 mM β-mercaptoethanol (Sigma) [33, 36, 37], and subsequently for 2 days in endothelial cell medium (EC; Life Technologies) supplemented with 2% B27 (Life Technologies), 20 ng/ml basic fibroblast growth factor (FGFb; Peprotech) and 10 µM retinoic acid (RA) [33, 36, 37]. Next, cells were singularised with StemPro™ Accutase (Gibco) and purified on collagen IV from human placenta (Sigma) and human plasma fibronectin (Life Technologies) coated plastic culture plates or 0.4–3.0 µm pore Transwell inserts (Corning Cat#CLS3412, Cat#CLS3415) as described previously [33, 34, 36, 37]. Following seeding densities were used in specified culture vessel formats: 24 well plate: 5×10^5 cells per well, 0.4 µm pore Transwell insert: 3×10^5 cells per Transwell, 3.0 µm pore Transwell insert: 4.5×10^5 cells per Transwell, as previously optimised by us and others [34, 36–40]. After one day, the medium was changed to EC+B27 (without FGFb and RA) to allow full cell maturation. All assays were performed 48 h following cell purification and iBECs were cultured in EC+B27 under normoxia (normoxia conditions (37 °C, 5% CO_2) for the duration of experimental assays [33, 36, 37]. For each iPSC line, iBECs from at least three independent iPSC differentiations were used in the experiments.

Differentiated iBECs were characterised for expression of BEC-specific markers occludin, claudin-5, ZO-1 and Glut-1 by immunofluorescence as previously described [33, 34, 36] utilising antibodies listed in Table S3. Image brightness was uniformly increased using ZEN Black Software (Zeiss) for presentation purposes.

To assess iBECs barrier integrity, cells were cultured on 24-well Transwell insert with 0.4 µm pore or 3.0 µm pore membrane (Corning) and transendothelial electrical resistance (TEER) across iBEC monolayer was measured with the EVOM3 Volt/Ohmmeter (World Precision Instruments) as previously described [33, 36]. TEER was measured in three areas per Transwell and the resistance of the blank (no-cells) Transwell was subtracted before averaging.

To assess the passive permeability of iBEC monolayer, cells were cultured in 0.4–3.0 µm pored Transwell inserts and fluorescein isothiocyanate (FITC)-conjugated dextran molecules of 3–5 kDa or 150 kDa (Sigma) were added at 0.5 mg/ml to the top chamber of the Transwell insert for 1–24 h as specified in the figure legend. Next, fluorescence signal intensity (490 nm excitation/520 nm emission) was measured in cell culture medium collected from the top and bottom chamber of the Transwell system (three technical replicates per Transwell) using a fluorescent plate reader (Biotek Synergy H4). Clearance volume describing dextran permeability was calculated as described previously by us and others [34, 36, 37] following the formula:

$$\text{Clearance volume} = \frac{\text{VB x (SB,t)}}{\text{ST, t}}$$

where VB is the volume of the bottom chamber (800 µl); SB, t is the signal of the bottom chamber at the time, t; ST, t is the signal of the top chamber at the time, t (1–24 h).

TDP-43 protein expression analysis

For immunofluorescence-based quantification of TDP-43 expression iBECs were purified on collagen IV and fibronectin-coated plastic coverslips at 5×10^5 cells per well in a 24 well plate. After one day, the medium was changed to EC+B27 (without FGFb and RA) and cells were allowed to mature for a further 24 h. 48 h following cell purification, iBECs were fixed with 4% paraformaldehyde (PFA) for 15 min at room temperature (RT). Next, cells were washed with PBS and permeabilised with 0.3% Triton X-100 for 10 min and blocked for 1 h at RT with 2% bovine serum albumin (BSA, Sigma)/2% normal goat

serum (GS, Chemicon) in PBS. Primary antibodies for TDP-43 (1:200) and ZO-1 (1:100) (Table S3) were diluted in a blocking solution and incubated with cells overnight at 4 °C. Then cells were washed with PBS and incubated with secondary antibodies (Table S3) diluted at 1:250 in a blocking solution for 1 h at RT. Subsequently, cells were washed with PBS and nuclear counterstaining was performed with Hoechst (1:5000). Coverslips were mounted with ProLong Gold Antifade (Invitrogen) and imaged at 100x magnification and identical image acquisition setting by the investigator blinded to cell genotype using a Zeiss 780 laser scanning confocal microscope. Antibody specificity was confirmed by performing secondary antibody-only controls.

Cytoplasmic and nuclear TDP-43 signal intensity (AU) in iBECs was measured in acquired images with ImageJ software, using methodology adapted from Quek et al. 2022 [41] where ZO-1 and Hoechst-stained cell images were used to create a mask for whole-cell and nucleus, respectively. Image contrast and brightness were uniformly increased using ZEN Black Software (Zeiss) for presentation purposes.

Rhodamine 123 accumulation assay

P-gp activity was measured using the intracellular accumulation of rhodamine 123, a known substrate of P-gp, in iBEC monolayers. This method, described previously [33, 38] [37, 42] was applied after iBECs were cultured on collagen IV and fibronectin for 48 h.

Initially, cells were treated with a P-gp inhibitor, Cyclosporin-A (CsA), at a concentration of 10 µM, or left untreated with only Hanks' balanced salt solution (HBSS), and incubated at 37 °C for 30 min. Subsequently, cells were exposed to 10 µM rhodamine 123 in the presence or absence of CsA in HBSS for 2 h at 37 °C. Following incubation, cells were rinsed with ice-cold Dulbecco's PBS (D-PBS) for 5 min and lysed using RIPA cell lysis buffer (Sigma) on a microplate shaker for 10 min. The fluorescence intensity of the cell lysates was measured using a Biotek Synergy H4 plate reader with excitation at 485 nm and emission at 530 nm. Results were normalized based on total protein content determined using a Pierce™ BCA protein assay kit (Thermo Fisher Scientific), following the manufacturer's instructions.

In the absence of CsA, rhodamine 123 is actively expelled from cells through the efflux function of P-gp. In contrast, inhibition of P-gp by CsA leads to increased intracellular accumulation of rhodamine 123. Therefore, higher levels of rhodamine 123 in cells treated with CsA indicate reduced P-gp activity. To quantify P-gp function, the fold change in rhodamine 123 uptake was calculated by comparing CsA-treated cells (+CsA) to untreated cells (-CsA) within each experimental group.

FUS^{+MB}-mediated delivery of 150 kDa dextran and anti-TDP-43 antibody

For ultrasound-mediated permeability studies, iBECs were cultured in Transwell inserts with 3.0 µm pores and exposed to FITC-conjugated 150 kDa dextran (0.5 mg/ml) or anti-TDP-43 antibody (1 µM, Sigma, Cat#T1705) and 10 µl of phospholipid-shelled microbubbles with octafluoropropane gas core prepared in-house as described in [43]. Wells were then immediately exposed to FUS at 286 kHz center frequency, 0.3 MPa peak rarefactional pressure, 50 cycles/burst, burst period 20 ms, and a 120 s sonication time as previously described [33, 36, 39]. 24 h following the treatment, cell culture medium was collected for dextran fluorescence signal intensity assessment as described above. Anti-TDP-43 antibody concentration was determined by Rabbit IgG enzyme-linked immunoassay kit (ELISA, Abcam) following manufacturer's instructions. For FUS^{+MB} studies, fold change in detected dextran clearance volume (calculated using the formula provided above) or antibody concentration was calculated relative to its untreated (UT) control for each line at 24 h.

Monolayer morphology assessment post FUS^{+MB}

To investigate potential mechanical damage of iBEC monolayer following FUS^{+MB} cells were cultured on collagen IV and fibronectin-coated plastic coverslips for 48 h and exposed to FUS at the parameters described above and 20 µl MB. Immediately (5 min) and 24 h post-treatment cells were fixed with 4% PFA for 15 min and immunofluorescence staining for ZO-1 was performed as described above. Coverslips were mounted with Dako Mounting medium (Agilent) and imaged at 20x magnification by the investigator blinded to the treatment condition using a Zeiss 780 confocal microscope. Image contrast and brightness were uniformly increased using ZEN Black Software (Zeiss) for presentation purposes.

Lactate dehydrogenase (LDH) viability assay

The effects of FUS^{+MB} on iBECs viability were assessed utilising CyQUANT LDH Cytotoxicity Assay (Thermo Fisher Scientific) as previously described [36]. Briefly, cells were cultured in 24-well plates and exposed to FUS at the parameters described above and 20 µl MB and cell culture media samples were collected immediately (30 min) and 24 h post-treatment. The levels of LDH enzyme were assessed with CyQUANT assay kit following manufacturer's instructions and calculated relative to its untreated (UT) control for each line [36].

iBEC monolayer integrity assessment post FUS^{+MB}

To assess the effects of FUS^{+MB} on iBEC monolayer integrity, iBECs were cultured on 3.0 µm pore Transwells and exposed FUS at the parameters described above

and 10 µl MB. TEER was measured immediately (1 h) and 24 h post-treatment in three areas per Transwell as described above and in [36]. Fold change in TEER compared to respective untreated (UT) controls was calculated.

RNA extraction, cDNA synthesis and quantitative real-time PCR (qPCR)

For cell phenotype characterisation, iPSC and iBEC were cultured under normal conditions and remained untreated prior to RNA collection. For FUS^{+MB} effects studies, cells were cultured in 24-well plates, exposed to FUS at the parameters described above and 20 µl MB, and cell RNA was collected immediately (30 min) and 24 h following FUS^{+MB} exposure as described [36].

For RNA collection, cells were rinsed with PBS and lysed in TRIzol™ reagent (ThermoFisher Scientific) and total RNA was extracted using the Direct-zol RNA Miniprep Kit (Zymo Research) according to the manufacturer's instructions. Isolated RNA quality and quantity was measured using NanoDrop™ Spectrophotometer. For quantitative real-time polymerase chain reaction (qPCR) studies, 150 ng of total RNA was converted to complementary DNA (cDNA) using SensiFAST™ cDNA synthesis kit following manufacturer instructions (Bioline) and qPCR performed in technical triplicate using SensiFAST™ SYBR® Lo-ROX Kit following manufacturer instructions (Bioline) on QuantStudio™ 5 Real-Time PCR system as previously described [33, 34, 36, 39]. Obtained Ct values were normalised by the Ct values of *18 S* endogenous control (ΔCt). Housekeeping gene expression of *18 S* was found to be consistent across cell lines. The ΔΔCt values were calculated as $2^{(-\Delta Ct)}$ and multiplied by 10^6. Technical triplicates were averaged per sample and log transformed for statistical analysis. Utilised primer sequences are presented in Table S4.

Statistical analysis

Statistical analysis was performed using GraphPad Prism version 9.4.0. For a two-group comparison with normal distribution, *F* test of equality of variances was performed and data was analysed with unpaired Student's *t*-test (two-tailed; data with equal variances) or unpaired Welch's *t*-test (two-tailed; data with unequal variances). When comparisons between three or more groups were analysed, one-way ANOVA followed by post-hoc tests were used. $P<0.05$ was considered statistically significant. Z-scores were calculated and values with Z-scores above or below two standard deviations (SD) of the mean were identified as outliers and excluded from analysis. Results are shown as mean±SEM. The number of independent (*n*) replicates used for each experiment is specified in figure legends. The number of technical replicates included in each assay is stated in the respective materials and methods sections.

Results

ALS iBECs demonstrate an altered phenotype compared to healthy donor controls

To study the ALS BBB in vitro, iBECs were generated human iBECs from a healthy donor (HD) iPSC line as previously characterised [33, 34] and two novel ALS iPSC lines derived from sporadic and familial (C9orf72 variant) ALS patients (Table S1, S2). The stemness of utilised iPSC lines was ascertained by the nuclear expression of SOX2 and Nanog proteins and iPSC-like morphology was confirmed by the formation of characteristic uniform colonies with defined edges (Figure S1A). Expression of pluripotency-regulator genes *SOX2*, *NANOG* and *OCT4* [44] was also confirmed at mRNA level and demonstrated no differences between control and ALS iPSCs, suggesting phenotypic similarity of selected iPSC lines (Figure S1B). The iPSCs were differentiated towards iBECs following previously published protocols [33, 34, 36] and successful generation of cells with brain endothelial-like phenotype confirmed by the formation of cobblestone-like monolayers and expression of BEC-associated markers including occludin, claudin-5, zonula occludens-1 (ZO-1) and glucose transporter-1 (Glut1) (Fig. 1A). When compared to parental iPSCs, mature iBECs presented decreased expression of pluripotency marker genes *SOX2*, *NANOG* and *OCT4* and a significant increase, or a trend towards an increase, in the expression of BEC-associated tight and adherens junction genes: occludin (*OCLN)*, claudin-5 (*CLDN5)*, ZO-1 (*TJP1)* and ve-cadherin (*CDH5)* (Figure S2), suggesting a switch towards the desired endothelial cell phenotype.

Since BBB pathology was previously described in ALS patients [15, 16, 24, 25], next was examined the development of a disease-related phenotype in generated patient-cell derived iBECs. Control and ALS cells cultured on traditionally used 0.4 µm pore Transwell inserts [33, 37, 40, 45] formed a confluent monolayer with transendothelial electrical resistance (TEER) corresponding to previously described iBEC models (34,35,38) (healthy donor: 4024±95.02, C9orf72 ALS: 2312±79.3, sporadic ALS: 1733±137.4 Ohm x cm^2, mean±SEM, Fig. 1B) confirming overall successful in vitro barrier formation. However, similar to BBB integrity impairment observed in ALS in vivo [19, 25], ALS iBECs generated a monolayer of reduced ($P<0.0001$) TEER compared to control cells, with sporadic ALS cells demonstrating lower ($P<0.01$) barrier integrity than C9orf72 expansion-carrying ALS iBECs (Fig. 1B). The passive permeability of iBEC monolayers to biologically inert 5 kDa dextran fluorescent tracer was assessed [36] and found to have increased leakage in C9orf72 ($P<0.0001$) and sporadic

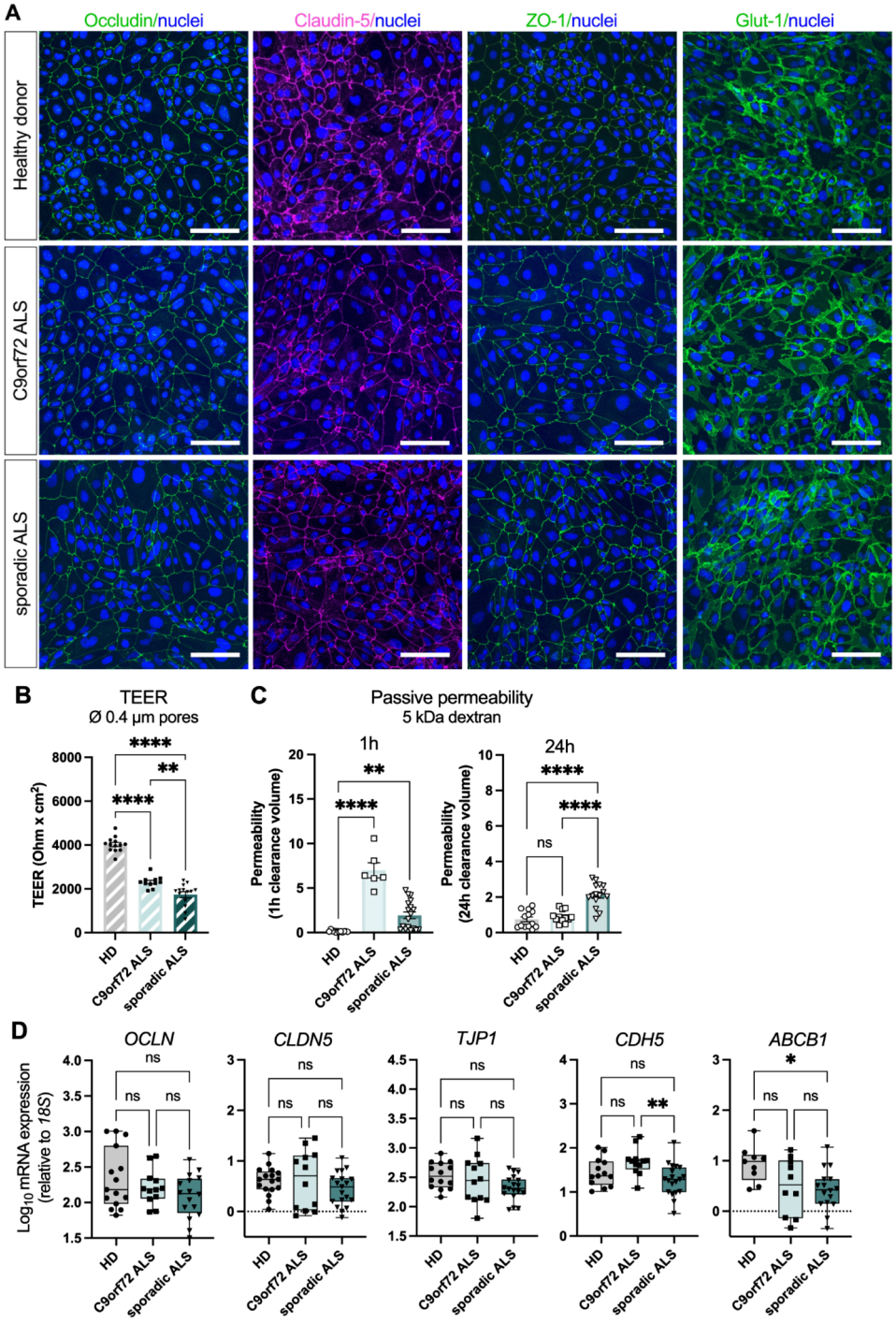

Fig. 1 Characterisation of brain endothelial-like cells (iBECs) generated from control and ALS human induced pluripotent stem cells (iPSCs). (**A**) Representative immunofluorescence images of occludin (green), claudin-5 (magenta), ZO-1 (green) and Glut-1 (green) with Hoechst nuclear counterstaining (blue) in healthy donor, C9orf72 ALS, and sporadic ALS iBECs. Scale bar = 100 µm. (**B**) Trans-endothelial electrical resistance (TEER, Ohm x cm^2) of a healthy donor, C9orf72 ALS, and sporadic ALS iBECs, measured in 0.4 µm pore Transwells. A minimum of $n = 11$ independent replicates per line. (**C**) Passive permeability of FITC-conjugated 5 kDa dextran in healthy donor, C9orf72 ALS, and sporadic ALS iBECs cultured on 0.4 µm pore Transwells assessed 1 h and 24 h following the addition of 5 kDa dextran. A minimum of $n = 6$ independent replicates per line. Data presented as clearance volume of dextran at 1 h and 24 h. (**D**) Relative mRNA expression of brain endothelial cell marker genes *OCLN*, *CLDN5*, *TJP1*, *CDH5* and *ABCB1* transporter in healthy donor, C9orf72 ALS, and sporadic ALS iBECs. Data presented as Log_{10} of ΔΔCT x 10^6, relative to *18 S*. A minimum of $n = 8$ independent replicates per line. Data in (B-D) analysed with One-way ANOVA with Tukey's test, error bars = SEM. *$P < 0.05$, **$P < 0.01$, ****$P < 0.0001$

ALS ($P<0.01$) iBECs compared to healthy donor controls when assessed 1 h post tracer addition, with this effect persisting in sporadic ALS iBECs ($P<0.0001$) when measured at 24 h time point (Fig. 1C). This was accompanied by downregulation ($P<0.01$) of *CDH5* mRNA expression in sporadic ALS iBECs (Fig. 1D); while the expression of tight junction markers *OCLN*, *CLDN5* and *TJP1* did not differ between control and ALS cells. Interestingly, the expression of *ABCB1* encoding for drug transporter P-gp was decreased ($P<0.05$) in sporadic ALS iBECs (Fig. 1D). When investigating the functional activity of P-gp via rhodamine accumulation, healthy donor and C9orf72 ALS iBECs demonstrated higher rhodamine uptake in the presence of the inhibitor (Figure S4A – B). However, no changes were observed in rhodamine uptake in sporadic ALS upon treatment with inihibitor (Figure S4C), suggesting that perhaps the low expression of ABCB1 correlates with reduced P-gp activity. These results are consistent with previous observations of P-gp dysregulation in ALS [13, 26, 46–48].

ALS iBECs reveal cytoplasmic accumulation of TDP-43 protein

TAR DNA-binding protein 43 (TDP-43) proteinopathy is a hallmark of ALS [49, 50] with TDP-43 protein aggregates recently being identified in cortical small blood vessels of sporadic ALS patients [51]. To investigate the potential TDP-43-related vasculopathy [51] in this model, the cellular localisation of TDP-43 protein in control and ALS iBECs by immunofluorescence was evaluated. Theanalysis revealed cytoplasmic accumulation of TDP-43 protein aggregates in ALS iBECs (Fig. 2A, Figure S3A) with both C9orf72 ($P<0.05$) and sporadic ($P<0.0001$) ALS cells demonstrating higher cytoplasmic TDP-43 protein signal intensity compared to healthy donor controls (Fig. 2B). Cytosolic TDP-43 aggregates were primarily granular in shape and more profound ($P<0.05$) in sporadic ALS as compared to C9orf72 ALS iBECs (Fig. 2A-B, Figure S3A). Interestingly, healthy donor iBECs presented low ($P<0.0001$) TDP-43 protein expression in the nucleus (compared to ALS cells), with no difference found in nuclear TDP-43 expression between sporadic and C9orf72 iBECs (Fig. 2B). Hence, to assess the distribution of total TDP-43 protein in studied cells, the ratio of cytoplasmic to nuclear TDP-43 signal was examined and revealed an increase in sporadic ALS iBECs compared to healthy donor controls ($P<0.05$) and C9orf72 ALS iBECs ($P<0.01$, Fig. 2C) corroborating TDP-43 mislocalisation in sporadic ALS cells. No signal was found in the secondary-only controls (Figure S3B) confirming the specificity of the utilised anti-TDP-43 antibody.

FUS^{+MB} facilitates controlled iBEC monolayer opening in vitro

It was previously demonstrated that FUS^{+MB} applied at clinically relevant [31, 52] parameters leads to reversible iBEC monolayer opening in familial and sporadic Alzheimer's disease (AD) BBB models [33, 36, 39]. In this study, characterised ALS patient-derived iBECs were used as a platform to investigate the FUS^{+MB}-mediated delivery of large molecule therapeutics at the ALS BBB.

Prior investigation revealed that most commonly used Transwell inserts with pores of 0.4 µm in diameter [33, 37, 40, 45, 53, 54] are not suitable to reliably assess the permeability of large (≥150 kDa) molecules and instead, Transwells with membranes containing 3.0 µm pores provide a technically advantageous alternative [36]. Hence, first was optimisation of ALS iBECs culture conditions leading to the development of a confluent cell barrier in Transwell inserts with 3.0 µm pores (Fig. 3A). As expected [55], control and ALS iBECs generated a barrier with lower TEER when cultured on 3.0 µm pored membranes as compared to the 0.4 µm Transwell (healthy donor: 1121±44.35, C9orf72 ALS: 845±42.61, sporadic ALS: 673±26.54 Ohm x cm^2, mean±SEM, Fig. 3B), while reaching 500 Ohm x cm^2 threshold ideal for assessing the passive penetration of small hydrophilic molecules [56]. Experiments performed in this Transwell format also replicated the reduced ($P<0.0001$) TEER in ALS iBECs compared to healthy donor cells, as well as a further decrease ($P<0.01$) in sporadic ALS iBECs TEER when compared to C9orf72 cells (Fig. 3B), corroborating previousfindings (Fig. 1B).

Utilising the 3.0 µm pore model, the effects of FUS^{+MB} on iBECs barrier integrity were examined. In clinical and animal studies FUS^{+MB} was shown to induce rapid BBB opening followed by full BBB integrity recovery within 24 h [27, 31, 52, 57]. Analogous to in vivo effects [27, 31, 52, 57], a significant decrease in TEER of healthy donor ($P<0.01$) and C9orf72 ALS ($P<0.05$) iBECs was found immediately (1 h) following FUS^{+MB} treatment (Fig. 3C). While achieving a similar fold reduction in TEER in healthy donor and C9orf72 ALS iBECs, statistically only a trend towards decreased TEER was found in sporadic ALS iBECs (healthy donor: 0.8905±0.02, C9orf72 ALS: 0.8803±0.03, sporadic ALS: 0.8565±0.04, mean±SEM fold change vs. respective untreated control, Fig. 3C, Figure S5A). This was also consistent with the estimated 10% reduction in TEER induced by 0.3 MPa FUS^{+MB} in other in vitro BBB studies [36, 58]. At 24 h following the treatment, no difference was found in TEER of sporadic ALS iBECs, while TEER was increased ($P<0.01$) in healthy donor and C9orf72 ALS iBECs (Fig. 3C, Figure S5A), corresponding to previous respective observations in sporadic [36] and familial [33] AD models. To confirm that changes in TEER were not resulting from cell death

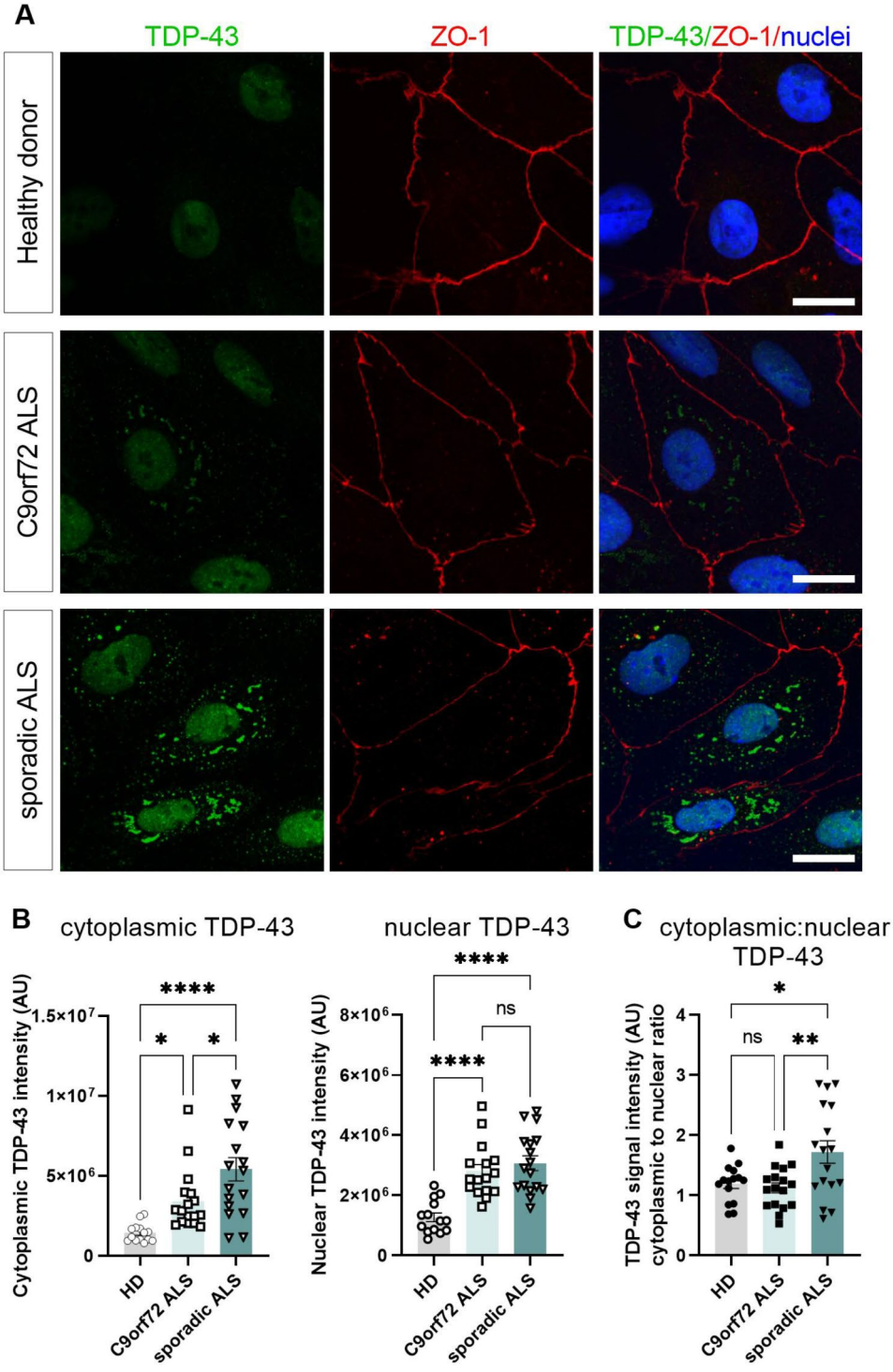

Fig. 2 Expression of TDP-43 protein in control and ALS iBECs. (**A**) Representative immunofluorescence images of TDP-43 (green) and ZO-1 (red) with Hoechst nuclear counterstaining (blue) in healthy donor, C9orf72 ALS, and sporadic ALS iBECs. Scale bar = 20 µm. (**B**) Comparison of TDP-43 signal intensity in the cytoplasm and nuclei of healthy donor, C9orf72 ALS, and sporadic ALS iBECs. (**C**) Comparison of cytoplasmic to nuclear TDP-43 signal intensity ratio in healthy donor, C9orf72 ALS, and sporadic ALS iBECs. A total of $n = 14–17$ cells analysed from four independent replicates per line in (**B**, **C**). Data in (**B**, **C**) analysed with One-way ANOVA with Tukey's test $^{*}P < 0.05$, $^{**}P < 0.01$, $^{****}P < 0.0001$, error bars = SEM

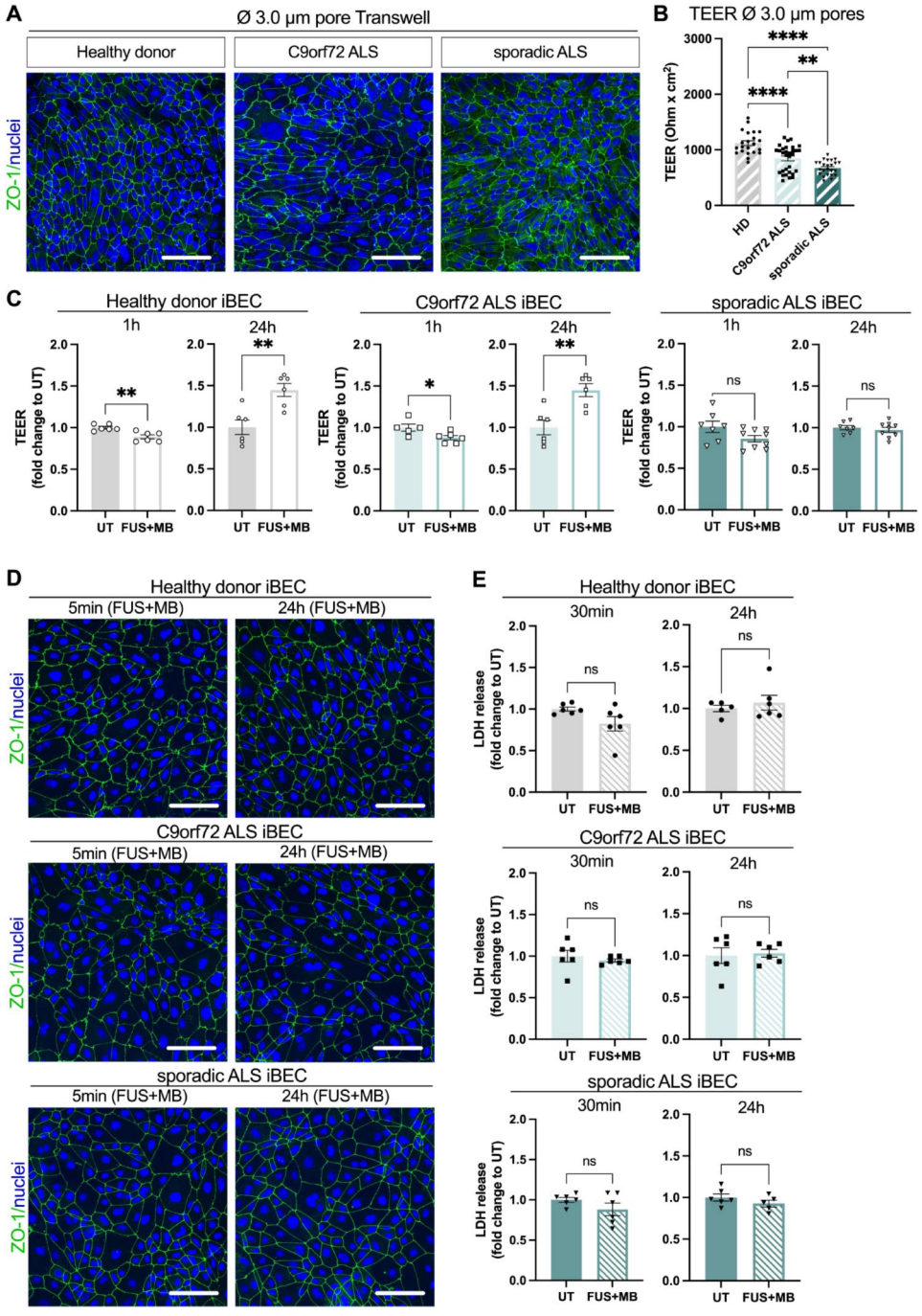

Fig. 3 Effects of FUS^{+MB} on viability and monolayer integrity of control and ALS iBECs. (**A**) Representative immunofluorescence images ZO-1 (green) with Hoechst nuclear counterstaining (blue) in healthy donor, C9orf72 ALS, and sporadic ALS iBECs cultured in 3.0 µm pore Transwell insert membrane. Scale bar = 100 µm. (**B**) Trans-endothelial electrical resistance (TEER, Ohm x cm^2) of healthy donor, C9orf72 ALS and sporadic ALS iBECs, measured in 3.0 µm pore Transwells. A minimum of $n = 22$ independent replicates per line. (**C**) Changes in TEER of healthy donor, C9orf72 ALS, and sporadic ALS iBECs exposed to FUS^{+MB}, 1 h and 24 h following the treatment. TEER was measured in 3.0 µm pore Transwells and shown as fold changes to untreated (UT) cells at respective time points. A minimum of $n = 5$ independent replicates per line. (**D**) Representative immunofluorescence images ZO-1 (green) with Hoechst nuclear counterstaining (blue) in healthy donor, C9orf72 ALS, and sporadic ALS iBECs exposed to FUS^{+MB}, shown immediately (5 min) and 24 h following the treatment. Cells were cultured on collagen IV and fibronectin-coated coverslips. Scale bar = 100 µm. (**E**) Changes in relative lactate dehydrogenase (LDH) release in healthy donor, C9orf72 ALS, and sporadic ALS iBECs exposed to FUS^{+MB}, 30 min and 24 h following the treatment. LDH release shown as fold changes to respective untreated (UT) cells at each time point. A minimum of $n = 5$ independent replicates per line. Data in (**B**) analysed with One-way ANOVA with Tukey's test, and in (**C**, **E**) with Student's *t*-test or Welch's *t*-test. Error bars = SEM. *$P < 0.05$, **$P < 0.01$, ***$P < 0.001$, ****$P < 0.0001$

induced by FUS^{+MB} iBECs viability was assessed following FUS^{+MB} exposure. The analysis revealed that FUS^{+MB} treatment did not cause any visible damage or morphology change in the control and ALS iBECs monolayer immediately (5 min) or 24 h post-treatment (Fig. 3D) and had no adverse effects on cell viability as assessed by lactate dehydrogenase (LDH) release assay at two time points tested (30 min and 24 h) (Fig. 3E). Relative LDH release also did not differ between the control and ALS lines immediately (30 min) and 24 h post FUS^{+MB} (Figure S5B).

FUS^{+MB} elicits differential molecular bioeffects in control and ALS iBECs

Although ultrasound-based ALS BBB opening technology is rapidly moving towards clinical use [31], the molecular responses of human ALS BBB cells to FUS^{+MB} remain unexplored. To further investigate the effects of FUS^{+MB} on control and ALS iBECs, cells were exposed to FUS^{+MB} and evaluated the resulting changes in gene expression at two time points corresponding to immediate iBEC monolayer opening (1 h) and its spontaneous recovery (24 h). Assuming that molecular changes would presume functional changes in monolayer integrity observed here as a decrease in TEER at 1 h post FUS^{+MB} (Fig. 3C), an earlier, 30 min time point was selected for gene expression studies.

Since FUS^{+MB} was previously shown to elicit molecular changes in tight and adherens junctions [33, 59] the expression of cell junction markers in iBECs via two-step reverse transcription quantitative polymerase chain reaction (RT-qPCR) was examined. When comparing to respective untreated cells, we found a significant decrease ($P<0.01$) in *OCLN* and *CDH5* expression in healthy donor iBECs immediately (30 min) post FUS^{+MB} while *OCLN* and *CLDN5* demonstrated reduced, ($P<0.05$) and *TJP1* increased, ($P<0.05$) expression in C9orf72 ALS iBECs (Fig. 4A, Figure S6). Interestingly, no changes in tight and adherens junction gene expression levels in sporadic ALS iBECs immediately (30 min) following FUS^{+MB} were found when compared to untreated cells from this line (Fig. 4A, Figure S6). Similarly, the expression of drug transporter *ABCB1* was not altered immediately (30 min) post FUS^{+MB} in healthy donor and ALS iBECs (Fig. 4A, Figure S6). However, when comparing between examined iBEC lines, differences in *OCLN*, *CLDN5*, *TJP1* and *CDH5* expression were found immediately (30 min) after FUS^{+MB} treatment collectively suggesting the molecular bioeffects of FUS^{+MB} may potentially impact different pathways in control and ALS cells (Fig. 4B).

24 h post FUS^{+MB}, tight and adherens junction gene expression normalised in healthy donor and C9orf72 ALS iBECs (Fig. 4C, Figure S6), suggesting iBEC monolayer recovery in these lines. Interestingly, at this time point, a significant increase in *CDH5* ($P<0.01$) and *ABCB1* ($P<0.05$) expression in sporadic ALS iBECs was found when compared to respective untreated cells (Fig. 4C, Figure S6). At 24 h, FUS^{+MB}-treated ALS iBECs also demonstrated increased expression of *CLDN5* as compared to healthy donor iBECs and higher expression of *CDH5* and *ABCB1* when compared to healthy donor and C9orf72 ALS cells (Fig. 4D), together indicating temporarily distinct responses of sporadic ALS iBECs to FUS^{+MB}.

FUS^{+MB}-mediated BBB opening was shown to remodel the immune landscape in the murine brain [60–64]. However, the neuroinflammatory responses to FUS^{+MB} of human ALS BBB cells are currently unknown. Thus, as both human primary BEC and iBECs have shown the capacity to elicit inflammatory responses [34, 65, 66], the expression of inflammatory mediators in FUS^{+MB}-treated iBECs was investigated. In this exploratory analysis inflammatory markers interleukin-6 (*IL6*), interleukin-8 (*IL8*), interleukin-1 A (*IL1A*), C-C motif chemokine ligand 2 (*CCL2*) and tumor necrosis factor-a (*TNF*) were selected as they were previously implicated in immune responses to FUS^{+MB} [36, 63, 64] and were shown to be expressed by iBECs [34].

Since neuroinflammation was linked with BBB pathology in ALS [21, 67], the baseline expression of inflammatory marker genes in untreated healthy donor and ALS iBECs was examined. Interstingly, while ALS is commonly associated with an increased proinflammatory profile [1, 23, 41, 68], a decreased ($P<0.05$) expression of proinflammatory marker genes, *IL6* and *TNF*, in sporadic ALS iBECs was found compared to healthy donor cells, with *IL6* demonstrating also reduced ($P<0.0001$) expression in sporadic ALS iBECs compared to C9orf72 ALS iBECs (Fig. 5A).

When assessing gene expression changes immediately (30 min) following FUS^{+MB}, decreased expression of *TNF* ($P<0.05$) in healthy donor cells as well as a decrease in *IL6* ($P<0.01$) and *CCL2* ($P<0.05$) in C9orf72 ALS iBECs was found suggesting potential immunosuppressive effect of FUS^{+MB} in these lines (Fig. 5B, Figure S7). Similar to the junctional markers, we found no changes in inflammatory marker gene expression in sporadic ALS iBECs immediately (30 min) post FUS^{+MB} (Fig. 5B, Figure S7). At 24 h, expression of *IL8* was reduced ($P<0.05$) in healthy donor iBECs while *IL6* showed increased ($P<0.05$) expression in sporadic ALS iBECs (Fig. 5D, Figure S7). When immediate responses were compared between independent lines, expression of *IL6* and *CCL2* was found to be decreased ($P<0.05$) in healthy donor and C9orf72 ALS iBECs compared to sporadic ALS iBECs while *TNF* showed increased ($P<0.05$) expression in C9orf72 iBECs compared to healthy donor control (Fig. 5C). Following 24 h, *IL6* and *TNF* expression were

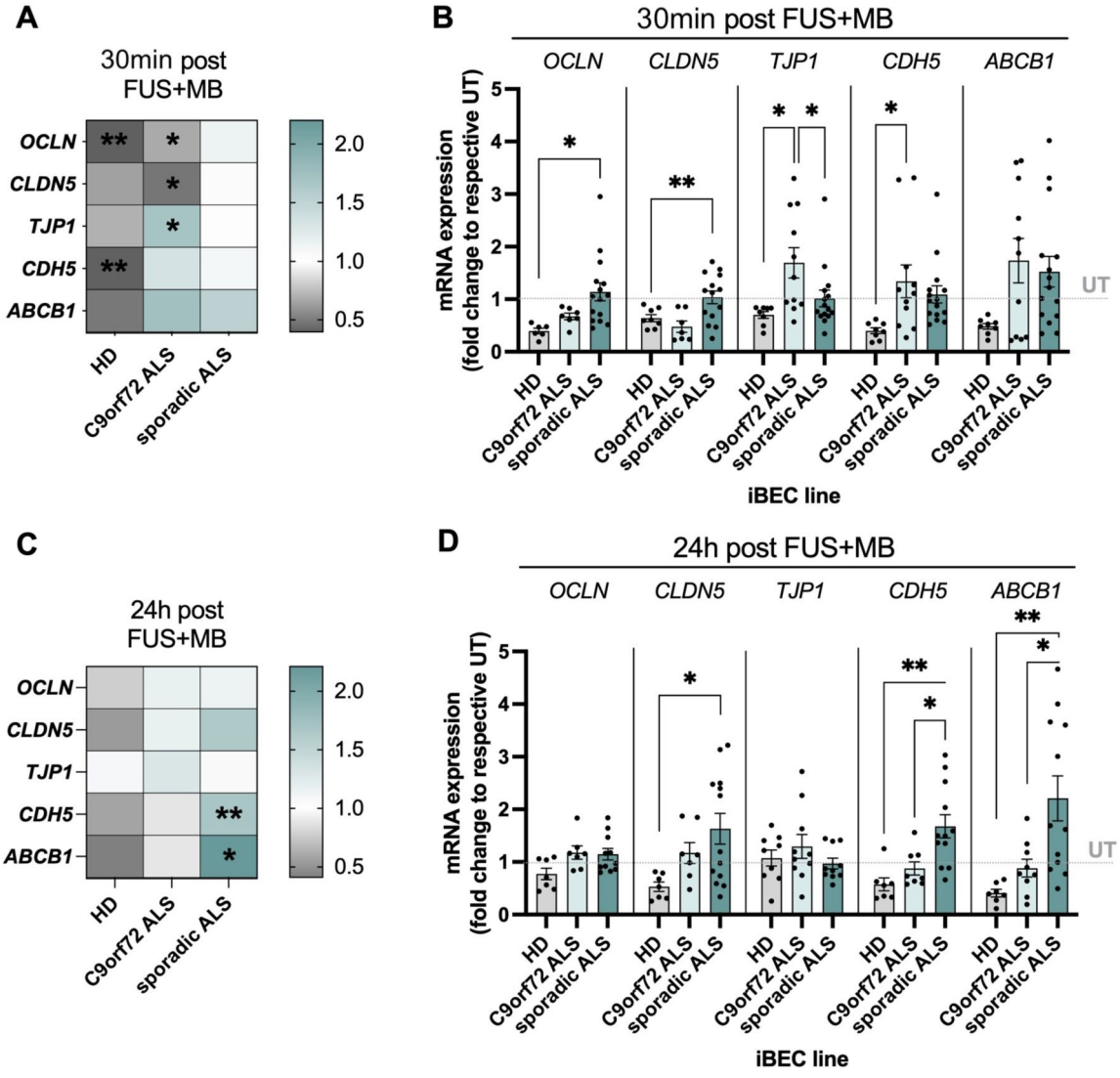

Fig. 4 Effects of FUS^{+MB} on the expression of junctional and transporter marker genes in control and ALS iBECs. (**A**, **C**) Heatmap summarising fold changes changes in mRNA expression of *OCLN*, *CLDN5*, *TJP1*, *CDH5*, *ABCB1* in healthy donor, C9orf72 ALS, and sporadic ALS iBECs exposed to FUS^{+MB}, 30 min (**A**) and 24 h (**C**) following the treatment. (**B**, **D**) Comparison of changes in mRNA expression of *OCLN*, *CLDN5*, *TJP1*, *CDH5*, *ABCB1* between healthy donor, C9orf72 ALS, and sporadic ALS iBEC, 30 min (**B**) and 24 h (**D**) following the FUS^{+MB} treatment. In **A-D**, a minimum of $n=6$ independent replicates per line. Data showed as fold changes to respective untreated (UT) cells from each cell group at each time point. Data in (**A**, **C**) analysed with Student's *t*-test or Welch's *t*-test and data in (**B**, **D**) analysed with One-way ANOVA with Tukey's test, error bars = SEM. Only significant changes are displayed in **A-D**. $^{*}P<0.05$, $^{**}P<0.01$

increased ($P<0.05$) in sporadic ALS iBECs compared to healthy donor cells and *CCL2* expression was reduced ($P<0.05$). Together, this differential gene expression may suggest that iBECs from each individual donor generate a unique and temporarily dynamic inflammatory profile in response to FUS^{+MB}.

FUS^{+MB} enhances anti-TDP-43 antibody permeability at ALS BBB in vitro

Different ALS drugs were successfully delivered across the BBB with FUS^{+MB} in the animal studies [28–30]. Yet, improving ALS drug delivery with FUS^{+MB} has not been trialled in the human ALS BBB in vitro or ALS patients. Here testing the delivery of a potentially therapeutic antibody in the ALS BBB model was performed given the previous broad preclinical success of antibody and FUS^{+MB} combined therapy [36, 39, 69–71] indicating high compatibility of ultrasound technique with this drug format. Due to the lack of immunotherapeutic agents approved for ALS, a commercially available anti-TDP-43 antibody was selected as a model molecule (~150 kDa) and developed a platform to trial its delivery with FUS^{+MB} in ALS iBECs (Fig. 6A).

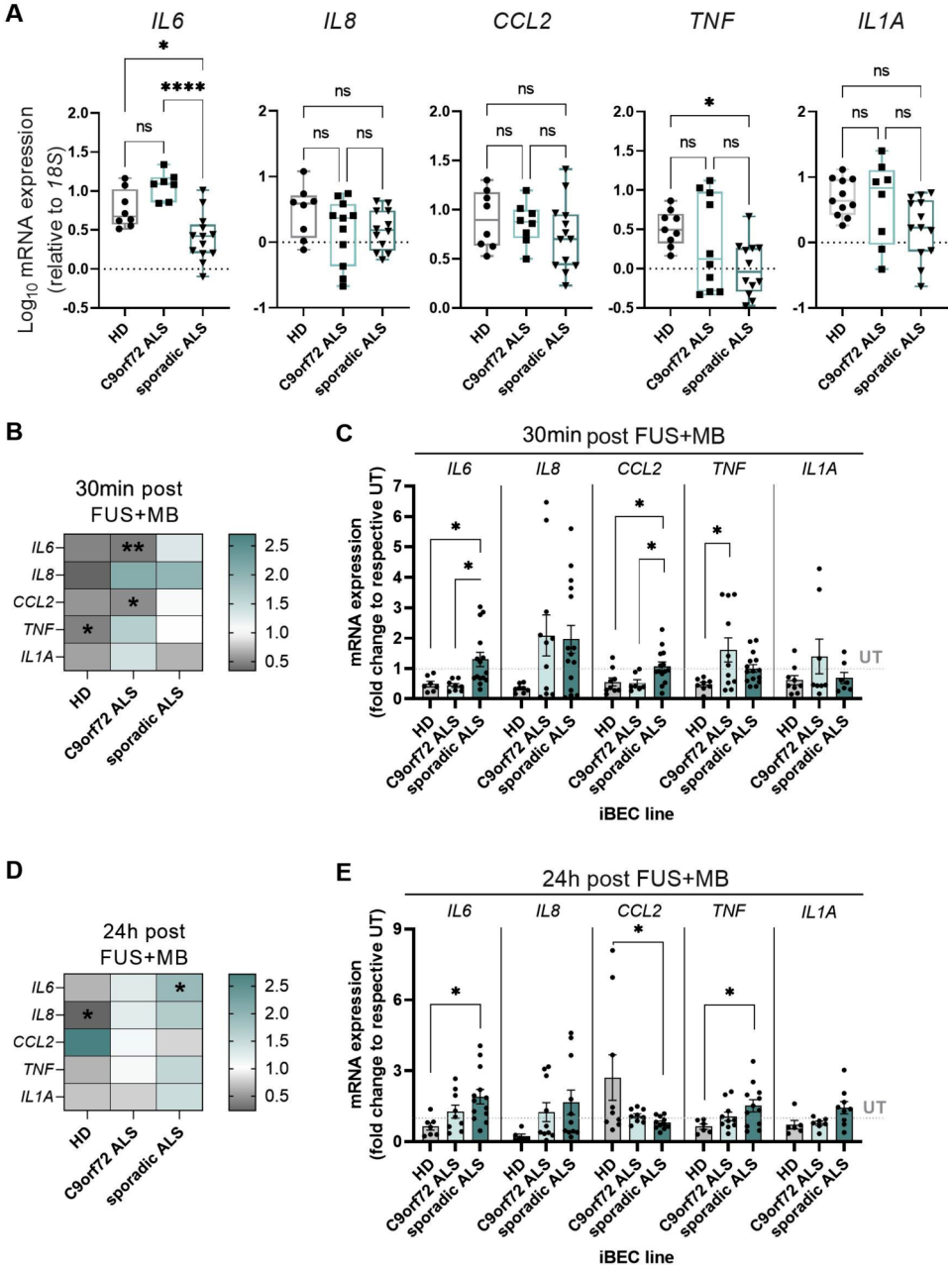

Fig. 5 Effects of FUS^{+MB} on the expression of inflammatory marker genes in control and ALS iBECs. (**A**) Relative mRNA expression of inflammatory marker genes *IL6*, *IL8*, *CCL2*, *TNF* and *IL1A* in the untreated healthy donor, C9orf72 ALS, and sporadic ALS iBECs. Data presented as Log_{10} of ΔΔCT x 10^6, relative to *18 S*. (**B**,**D**) Heatmap summarising fold changes in mRNA expression of *IL6*, *IL8*, *CCL2*, *TNF* and *IL1A* in healthy donor, C9orf72 ALS, and sporadic ALS iBEC exposed to FUS^{+MB}, 30 min (**B**) and 24 h (**D**) following the treatment. (**C**, **E**) Comparison of changes in mRNA expression of *IL6*, *IL8*, *CCL2*, *TNF* and *IL1A* between healthy donor, C9orf72 ALS, and sporadic ALS iBECs, 30 min (**C**) and 24 h (**E**) following the FUS^{+MB} treatment. In A-E, a minimum of $n = 6$ independent replicates per line. Data in (**B-E**) showed as fold changes to respective untreated (UT) cells from each cell group at each time point. Data in (**B**, **D**) analysed with Student's *t*-test or Welch's *t*-test and data in (**A**, **C**, **E**) analysed with One-way ANOVA with Tukey's test, error bars = SEM. Only significant changes are displayed in B-E. *$P < 0.05$, **$P < 0.01$, ****$P < 0.0001$

First, the passive transport of large molecules in ALS iBECs was explored by studying the permeability of a biologically inert 150 kDa dextran fluorescent tracer. Similar to the 5 kDa tracer permeability at 24 h (Fig. 1C), increased leakage of 150 kDa dextran in sporadic ALS iBECs was found compared to healthy donor ($P<0.0001$) and C9orf72 ALS ($P<0.01$) iBECs (Fig. 6B). This suggests that the sporadic ALS cells consistently demonstrate iBECs permeability impairment at this time point. Next, cells were cultured on 3.0 µm pore Transwells and exposed to FUS^{+MB} together with 150 kDa dextran and its permeability was assessed at 24 h post-treatment as

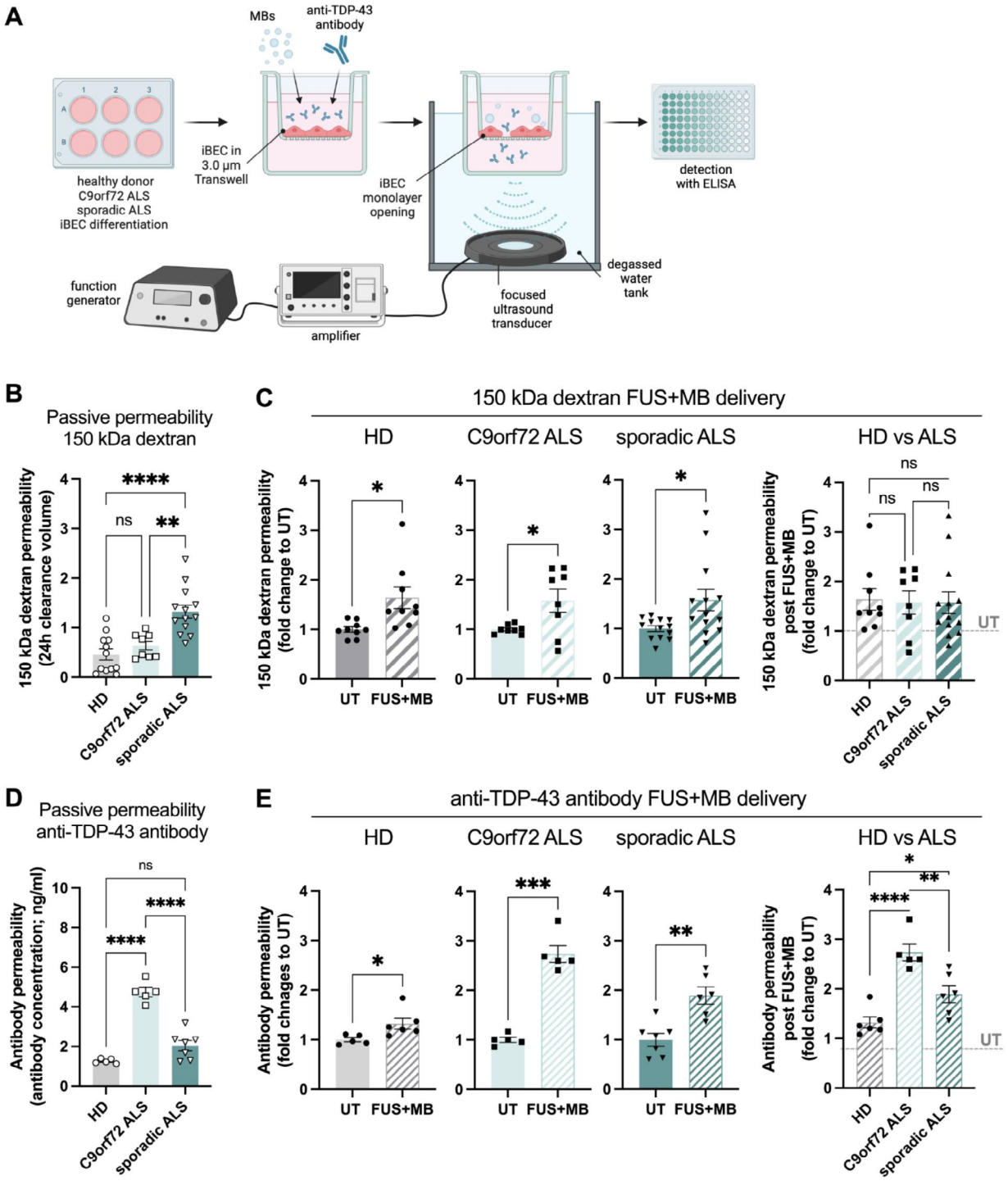

Fig. 6 FUS^{+MB}-mediated delivery of 150 kDa dextran and anti-TDP-43 antibody in control and ALS iBECs. (**A**) Schematic illustration of FUS^{+MB} mediated anti-TDP-43 antibody delivery in the Transwell model. (**B**) Passive permeability of 150 kDa dextran in healthy donor, C9orf72 ALS, and sporadic ALS iBECs cultured in 3.0 µm poreTranswell. A minimum of $n = 8$ independent replicates per line. Data presented as clearance volume of dextran at 24 h. (**C**) Delivery of 150 kDa dextran in healthy donor, C9orf72 ALS, and sporadic ALS iBECs using FUS^{+MB}. Permeability shown as fold change to respective untrated (UT) cells at 24 h. A minimum of $n = 8$ independent replicates per line. (**D**) Passive permeability of anti-TDP-43 antibody in healthy donor, C9orf72 ALS, and sporadic ALS iBECs cultured in 3.0 µm pore Transwell. A minimum of $n = 5$ independent replicates per line. Data presented as anti-TDP-43 IgG concentration (ng/ml) detected in the bottom of the Transwell at 24 h. (**E**) Delivery of anti-TDP-43 antibody in healthy donor, C9orf72 ALS, and sporadic ALS iBECs using FUS^{+MB}. Permeability shown as fold change to respective untrated (UT) cells at 24 h. A minimum of $n = 5$ independent replicates per line. Data in (**B**, **D**) and three-group comparison in (**C**, **E**) analysed with with One-way ANOVA with Tukey's test. Two-group comparisons in (**C**, **E**) analysed with Student's *t*-test or Welch's *t*-test. *$P < 0.05$, **$P < 0.01$, ***$P < 0.001$, ****$P < 0.0001$, error bars = SEM

previously described [36]. Similar to previous observations in the AD model [36], we found FUS^{+MB} to increase ($P<0.05$) 150 kDa dextran delivery in iBECs with no differences in delivery efficiency between control and ALS lines (Fig. 6C).

Interestingly, when the permeability of anti-TDP-43 antibody was assessed without FUS^{+MB}, increased ($P<0.0001$) penetration was identified in C9orf72 ALS iBECs, compared to healthy donor and sporadic ALS iBECs (Fig. 6D), with this effect not directly corresponding to C9orf72 ALS iBEC monolayer TEER (Fig. 3B) or permeability to 150 kDa dextran (Fig. 6B). Next anti-TDP-43 antibody delivery with FUS^{+MB} was trialled and increased permeability was found in healthy donor ($P<0.05$), C9orf72 ALS ($P<0.001$) and sporadic ALS ($P<0.01$) iBECs (Fig. 6E). Analogous to antibody penetration without FUS^{+MB} treatment, FUS^{+MB}-enhanced anti-TDP-43 antibody delivery efficiency proved to be the highest in C9orf72 ALS iBECs ($P<0.0001$ vs. HD iBECs and $P<0.01$ vs. sporadic ALS iBECs, Fig. 6E). Importantly, a higher fold permeability increase ($P<0.05$) was also found in sporadic ALS iBECs compared to healthy donor cells (Fig. 6E), collectively suggesting the high efficiency of anti-TDP-43 antibody delivery with FUS^{+MB} in ALS models. Furthermore, despite BBB integrity changes not being detectable with TEER technique in sporadic ALS iBECs (Fig. 3C), observation of increased permeability of 150 kDa dextran and anti-TDP-43 antibody confirmed effective monolayer opening in ALS iBECs following FUS^{+MB}.

Discussion

ALS is a fatal neurodegenerative condition with approved treatment options being limited to riluzole [72], edaravone [73] and tofersen antisense oligonucleotide [10, 74] therapies. Their effectiveness however is restricted by the pharmacoresistance of the BBB [10, 74–77] warranting the development of non-invasive drug delivery technologies that could maximise the amount of drug reaching its CNS target. FUS^{+MB} is a promising technique facilitating temporary BBB opening [27] with its clinical safety and effectiveness in ALS confirmed by a pioneering study [31]. While reversibly increasing the permeabilisation of the BBB to applied drugs in animal studies [28–30], FUS^{+MB} has not yet been combined with any therapeutic molecule in ALS patients.

Here, an ALS patient-cell-derived in vitro platform was developed to screen for the molecular and cellular bioeffects of FUS^{+MB} and provide the first proof-of-concept evidence for the feasibility of FUS^{+MB} to enhance large molecule drug delivery at human ALS BBB. By utilising sporadic and familial (*C9orf72* expansion variant) ALS iBECs as a BBB model, it was found that phenotypical differences in ALS iBECs integrity, permeability, intracellular TDP-43 protein localisation, junctional marker and drug transporter expression occurred, replicating some of the hallmark disease-associated changes at BBB in ALS [15, 16]. Interestingly, familial ALS cells were obtained from asymptomatic (at the time of skin biopsy) *C9orf72* expansion carrier who experienced disease onset later in life, suggesting these BBB changes may precede clinical ALS symptoms development in *C9orf72*-dependent ALS. Notably, differences in integrity and permeability did not closely match expression levels of major tight junction proteins in the different cell-lines (as shown in Fig. 1). This is not unexpected as many other membrane components can also affect barrier integrity [78]. A further in-depth study of these components in the future may reveal alternative differences in protein, lipid or extracellular matrix components between the HD and ALS cell lines that could support the altered integrity.

This exploratory analysis further revealed that FUS^{+MB} elicits temporary changes in ALS iBEC monolayer integrity and permeability to fluorescent 150 kDa tracer with no adverse effects on cell viability or morphology. It is also the first to demonstrate improved transport of anti-TDP-43 antibody in ALS iBECs following FUS^{+MB} exposure. These effects were accompanied by molecular changes in junctional protein, drug transporter and inflammatory marker gene expression in ALS iBECs providing first insights into the cell-specific responses of human BBB cells to FUS^{+MB}. With the model recapitulating aspects of clinical BBB phenotype in ALS [15, 16, 24], observed effects would prove to be of high translational relevance and support future clinical success of FUS^{+MB} mediated drug delivery in ALS patients.

Extensive evidence suggests BBB impairment in the ALS [15, 16, 19, 25, 51]. However, with important discrepancies found in BBB pathology between ALS animal models and patients [24], it remains critical to develop fully human in vitro BBB models facilitating understanding of BBB changes in ALS. iPSC-derived iBECs [37, 45, 53] serve as key cellular component of human BBB models, offering currently the highest drug permeability mimicry when compared to the human in vivo brain [79, 80]. Despite the importance of BBB modelling in ALS, studies describing iBECs generation from ALS patient iPSCs are sparse and limited to its familial form [56]. The phenotypic characterisation of human ALS iBECs revealed a decrease in TEER of monolayers formed by ALS cells, suggesting barrier integrity impairment in the disease, previously also reported for SOD1 mutation and *C9orf72* expansion carrying iBECs [56]. It has also been shown that the barrier integrity is lower in sporadic ALS iBECs as compared to C9orf72 iBECs and accompanied by increased passive permeability to 5 kDa and 150 kDa fluorescent tracers, pointing to potential phenotypic

heterogeneity between disease subtypes. This could also explain inconsistent results of clinical reports where BBB disruption was found only in a fraction of ALS patients [81–84], highlighting the need for more careful patient stratification in generalised cohort studies.

Interestingly, it was also found that sporadic ALS iBECs express lower levels of *CDH5* encoding for adherens junction complex protein VE-cadherin, previously shown to govern endothelium permeability [85]. With no changes observed in tight junction-associated genes, these results could indicate specific vulnerability of adherens junction complexes in sporadic ALS, warranting its further validation at protein and functional levels. Furthermore, in contrast to previous in vivo studies [13, 47], experiments performed in the model identified reduced expression of *ABCB1* in sporadic ALS iBECs with its expression not being altered in C9orf72 ALS iBECs, and when investigating the functional activity of P-gp, reduced activity of P-gp in sporadic ALS iBECs was found. This however was partially aligned with an in vitro study where P-gp activity was shown to be decreased in *C9orf72* expansion carrying iBECs [56], together supporting overall P-gp dysregulation in ALS.

TDP-43 protein pathology can be found in almost all ALS cases where it is primarily linked to motor neuron degeneration [86, 87]. Interestingly, TDP-43 and phosphorylated TDP-43 aggregates were recently found in cortical vessel walls of sporadic ALS patients [51]. However, with BBB comprising multiple cell types, an association of TDP-43 with specific cell type within the neurovascular unit was not determined [51]. Similarly, the source (endogenous vs. neuron-derived) of TDP-43 protein aggregates at the blood vessels was not examined and the brain endothelial cell-type-specific effects of TDP-43 proteinopathy are not clear.

Here, it was found that cytoplasmic TDP-43 protein aggregates occurred in a single-cell-type ALS iBECs culture. This was accompanied by the disease-associated changes in ALS iBECs with the degree of TEER and permeability impairment being proportional to the amount of TDP-43 aggregates found in C9orf72 and sporadic ALS cells. Although further investigation is required, the observation suggests that endogenous TDP-43 proteinopathy may be present in BECs and influence cerebrovascular homeostasis in the disease. Importantly, however, iPSCs utilised in this study were reprogrammed from skin fibroblasts of a healthy donor [33] and ALS patients, and cytoplasmic mislocalisation and accumulation of TDP-43 was recently reported in human ALS fibroblasts [88–90]. Hence TDP-43 pathology could also be carried from source fibroblasts, warranting further validation of previousin vitro results in human ALS brain tissue.

When assessing the passive transport (without FUS^{+MB}) of molecules in the ALS mode,l increased permeability of biologically inert 5 kDa and 150 kDa dextran in sporadic ALS iBECs was found, consistent with the lowest TEER generated by this line. However, anti-TDP-43 antibody leakage was the highest in C9orf72 ALS cells, with C9orf72 ALS iBECs demonstrating higher barrier integrity and simultaneously lower cytoplasmic TPD-43 protein content than sporadic ALS iBECs. This may suggest that the permeability of potentially therapeutic antibodies in ALS iBECs is not dependent on the net barrier integrity, but rather, points to the complex molecular interactions of antibodies with patient-derived cells; mimicking previousfindings for anti-tau antibodies in the sporadic AD model [39]. Observed effects may also imply the heterogeneity in drug permeability routes at barriers of sporadic and familial ALS patient subtypes and highlight alterations in paracellular and transcellular BBB transport pathways in ALS. This could also explain the lack of widespread drug permeability at seemingly more leaky BBB in ALS [91] since all three approved treatments [13, 74] require at least in part transcellular transport mechanisms.

Given the need for improving drug delivery at the ALS BBB [91] and the lack of fully human in vitro models allowing for investigation of FUS^{+MB} effects on ALS BBB cells, characterised ALS iBECs were utilized to develop a FUS^{+MB}-mediated drug permeability screening platform. Correlating with the clinical ALS study [31], the analysis confirmed the transient effect of FUS^{+MB} on iBEC monolayer opening, as reflected by a reduction in TEER immediately following the treatment. While no changes were found in the integrity of sporadic ALS iBECs 24 h post-treatment, the TEER of healthy donor control and familial C9orf72 ALS iBECs was increased as compared to untreated cells at this time point. Interestingly, in previous studies with sporadic [36] and familial [33] AD models, it was also found that a consistent decrease in barrier integrity occurred immediately following FUS^{+MB}; whereas the TEER was no longer altered at 24 h post FUS^{+MB} in the sporadic AD model, but increased in familial AD iBECs, mirroring respective observations in sporadic and familial ALS cells. Together this could suggest some cellular responses to FUS^{+MB} could be shared between familial and sporadic variants of neurodegenerative diseases warranting further investigation.

RNA sequencing was previously performed in sporadic AD iBECs exposed to FUS^{+MB} and reported no differences in gene expression immediately and 24 h post-treatment [36]. Previous analysis conducted by qPCR demonstrated FUS^{+MB}-induced changes in *OCLN*, *CLDN5*, *TJP1* and *CDH5* expression in familial AD iBECs [33]. In this study, when considering FUS^{+MB} elicited molecular effects in ALS cells, expression of the same

junctional marker genes was found to be altered in iBECs. However, this was limited to healthy donor and C9orf72 cells, with sporadic ALS iBECs showing no response to FUS^{+MB} immediately following the treatment. Sporadic ALS iBECs proved to be more responsive at 24 h timepoint presenting altered *CDH5* expression levels. Previous analysis also revealed a trend towards decreased expression of P-gp-encoding *ABCB1* in healthy donor cells and contrarily increased expression in sporadic ALS iBECs following FUS^{+MB}, supporting previously reported modulatory effects of FUS^{+MB} on drug transporter expression and function in AD iBECs [38]. With P-gp serving as a major drug efflux transporter at the BBB, its elevated activity could prove to be counteractive to FUS^{+MB}-mediated drug delivery and confer CNS pharmacoresistance in sporadic ALS. While requiring validation at protein and functional levels, further investigation in the ALS model could aid in the early identification of such responses and test for strategies [13] mitigating undesired effects of FUS^{+MB} in defined subpopulations of patients.

FUS^{+MB} was previously shown to induce neuroinflammatory responses in animal studies [63, 64, 92] motivating exploratory analysis of selected proinflammatory marker expression in ALS iBECs. Intriguingly, reduced expression of *TNF* and *IL8* in healthy donor cells, and *IL6* and *CCL2* in C9orf72 ALS iBECs was identified, suggesting FUS^{+MB} may rather confer immunosuppressive effects in cells of some individuals. Sporadic ALS iBECs showed a differential expression profile, presenting the increased expression of *IL6* and *CCL2* at the immediate time point and *IL6* and *TNF* at 24 h when compared to other lines, but overall lacked a profound proinflammatory response to FUS^{+MB}. These observations were consistent with a previous study [36] showing no change or decreased proinflammatory marker gene expression in sporadic AD iPSC-derived iAstrocytes exposed to FUS^{+MB}. While in vivo responses in the human brain are still unexplored, this could point to potential discrepancies in neuroinflammatory effects of FUS^{+MB} between animal and human cells, warranting future evaluation of a larger library of inflammatory markers expression at both gene and protein levels in the presented here human ALS in vitro BBB models.

With BBB limiting an estimated 99.8% of peripherally administered large molecule drugs such as therapeutics antibodies [93], the possibility of enhancing the permeabilisation of ALS BBB to large molecules with FUS^{+MB} was tested. As a proof-of-concept, we trialled the delivery of anti-TDP-43 antibody, considering promising preclinical development of TDP-43 targeted immunotherapies [94–97] as well as the recent clinical success of therapeutic antibodies in the treatment of other neurodegenerative disorders [98–102]. Although the utilised anti-TDP-43 antibody has not yet proved therapeutically beneficial, previous success in delivering Aducanumab (Aduhelm™) and anti-tau therapeutic antibodies with FUS^{+MB} in human Alzheimer's disease in vitro models has been reported [36, 39]; and a recent clinical study demonstrated beneficial effects of Aducanumab combined with FUS^{+MB} in Alzheimer's disease patients, as compared to Aducanumab alone [102]. Hence, it was hypothesised that analogously, achieving increased permeability of this model anti-TDP-43 antibody in the cell platform could be representative of future clinically approved ALS immunotherapeutics.

Here, it was demonstrated for the first time that FUS^{+MB} facilitates improved permeability of anti-TDP-43 antibody at ALS BBB in vitro. Interestingly, antibody delivery efficiency was higher in C9orf72 and sporadic ALS iBECs than control cells, reaching 2.7- and 1.9-fold increases respectively, as compared to its passive permeability, suggesting potential for promising drug delivery enhancement in ALS. While improving the cost-effectiveness of immunotherapy, it remains to be determined whether such improvement in drug delivery would be therapeutically meaningful in patients. However, a 2-fold increase in edaravone permeability following FUS^{+MB} was associated with additional symptom amelioration in an ALS mouse model [29], suggesting it is a sufficient increase to enhance therapeutic outcomes. In the future, further increase in drug permeability can be achieved in combination with currently preclinically investigated tight junction binders which were shown to improve BBB opening with FUS^{+MB}, expanding the therapeutic window for drug application [58].

While providing an advancement in FUS^{+MB} drug delivery in ALS, there are several limitations to this study. Firstly, these observations should be confirmed with an increased number of iPSC lines [103] to account for broader heterogeneity in sporadic and familial ALS patient populations, and improve the translatability of the findings. Additionally, in comparison to primary human BECs, iPSC-derived iBECs are known to carry elements of epithelial transcriptomic signature [54], warranting further improvements in iBEC differentiation protocols to achieve utmost human BEC mimicry in ALS iPSC-derived models. Given the extensive role of other neurovascular unit cells such as pericytes and astrocytes in regulating BBB permeability [104–107], future development of multicellular and 3D models [36, 108] is needed to further aid in understanding FUS^{+MB} effects on the human BBB in ALS.

Finally, the BBB is not the only barrier limiting drug delivery into the CNS and the blood-spinal cord barrier (BSCB) – formed by BSCB-specific endothelium, astrocytes and pericytes - is also a known contributor to pharmacoresistance in ALS [16, 17]. While sharing

morphological and functional characteristics with the BBB, BSCB's BECs express reduced levels of junctional proteins (ZO-1, occludin, b-catenin, VE-cadherin) and P-gp, resulting in the higher vulnerability of BSCB to pro-inflammatory cytokines and toxin infiltration [16, 17, 24, 109]. Changes in TJ expression, mitochondrial dysfunction, and impaired endothelium repair were also found in the BEC at the BSCB of ALS patients, contributing to vascular-mediated neurodegeneration and disease progression [17, 110, 111]. Although FUS^{+MB}-mediated BSCB opening and drug delivery into the spinal cord have been successfully performed in non-ALS rodents [112–114], this technique has not yet been used clinically in humans. Therefore, in the current study, the development of the BBB model for FUS^{+MB} mediated drug screening in ALS was investigated as this technology can be more rapidly delivered to patients. However, future in vitro BSCB modelling and FUS^{+MB}-mediated drug delivery screening would be a significant advancement in understanding blood-CNS barriers' impairment and overcoming pharmacoresistance in ALS.

Together these results provide important proof-of-concept evidence for non-invasive, FUS^{+MB}-facilitated antibody transport across the in vitro ALS BBB, which could aid in improving the delivery of large molecule drugs and TDP-43-directed immunotherapies [94–97] in ALS. With no such platform reported to date, the study provides the first patient-cell-derived model for investigation of FUS^{+MB} bioeffects and screening of FUS^{+MB}-deliverable drug formats most compatible with disease subtypes, supporting personalised medicine approaches to ALS drug delivery.

Conclusions

The BBB restricts the entry of large-molecule drugs into the brain, limiting treatment effectiveness in ALS. The study presents a novel ALS patient-derived blood-brain barrier (BBB) cell platform for the advancement of FUS^{+MB}-mediated drug delivery and demonstrates for the first time that FUS^{+MB} increases the delivery of potentially therapeutic anti-TDP-43 antibody across the in vitro barrier. These findings are an important step in accelerating the translation of FUS^{+MB} as a CNS drug delivery technology in the treatment of ALS, especially in conjunction with immunotherapeutics.

Abbreviations

ALS	Amyotrophic lateral sclerosis
AD	Alzheimer's disease
BBB	Blood-brain barrier
BEC	Brain endothelial cell
BSCB	Blood-spinal cord barrier
CNS	Central nervous system
ELISA	Enzyme-linked immunosorbent assay
FUS	Focused ultrasound
HD	Healthy donor
iBEC	induced brain endothelial-like cell
Imm	Immediately
iPSC	induced pluripotent stem cell
MB	Microbubble
qPCR	quantitative polymerase chain reaction
TDP-43	TAR DNA-binding protein 43
TEER	Trans-endothelial electrical resistance
UT	Untreated

Supplementary Information

The online version contains supplementary material available at https://doi.org/10.1186/s12987-024-00565-1.

Supplementary Material 1

Acknowledgements

We thank QIMR Berghofer MRI Flow Cytometry and Imaging Facility for their assistance and Dr Satomi Okano and QIMR Berghofer MRI Statistics department for their advice on data analysis. We thank prof. Jose M. Polo (Monash University) for the provision of HDFa hiPSC line. Graphical elements were generated with Biorender.com.

Author contributions

JMW: conceptualisation, methodology, investigation, formal analysis, visualisation, writing - original draft, writing - review & editing; JDSC: methodology, investigation, formal analysis, visualisation, writing - review & editing; MCC: methodology; MP: methodology; SV: methodology; THN: methodology; VLB: conceptualisation, methodology, resources; LEO: methodology; LO: conceptualisation, methodology, resources; ARW: conceptualisation, writing - review & editing, supervision, project administration, funding acquisition. All authors reviewed and approved the final manuscript.

Funding

This work was supported by: FightMND, NHMRC Project grant APP1125796 (ARW), National Health and Medical Research Council (NHMRC) Senior Research Fellowship (1118452) (ARW). JMW was a recipient of The University of Queensland PhD scholarship and QIMR Berghofer Medical Research Institute Top-Up Scholarship.

Data availability

The datasets supporting the conclusions of this article are included within the article and its additional file and are available from the corresponding author upon reasonable request.

Declarations

Ethics approval

The study was approved by the University of Palermo Ethics Committee (Palermo 1, n° 4/2019), the University of Wollongong Human Research Ethics Committee (18/366) and QIMR Berghofer Human Ethics Committee (P2197). All participants provided informed consent before participating in the study.

Consent for publication

Not applicable.

Competing interests

The authors declare no competing interests.

Author details

[1]Brain and Mental Health Program, QIMR Berghofer Medical Research Institute, Brisbane, QLD, Australia
[2]Faculty of Medicine, University of Queensland, St. Lucia, QLD, Australia
[3]Molecular Horizons, School of Chemistry and Molecular Bioscience, University of Wollongong, Northfields Avenue, Wollongong, NSW, Australia
[4]The Novo Nordisk Foundation Center for Stem Cell Medicine (reNEW), Murdoch Children's Research Institute (MCRI), Parkville, VIC, Australia

[5]ALS Clinical Research Centre and Laboratory of Neurochemistry, Department of Biomedicine, Neurosciences and Advanced Diagnosis, University of Palermo, Palermo, Italy
[6]Flow Cytometry and Imaging Facility, QIMR Berghofer Medical Research Institute, Brisbane, QLD, Australia
[7]School of Biomedical Sciences, Faculty of Health, Queensland University of Technology, Brisbane, QLD, Australia
[8]School of Biomedical Science, University of Queensland, St. Lucia, QLD, Australia
[9]A.I. Virtanen Institute for Molecular Sciences, University of Eastern Finland, Kuopio, Finland

Received: 28 February 2024 / Accepted: 6 August 2024
Published online: 13 August 2024

References

1. Mead RJ, Shan N, Reiser HJ, Marshall F, Shaw PJ. Amyotrophic lateral sclerosis: a neurodegenerative disorder poised for successful therapeutic translation. Nat Rev Drug Discov. 2023;22(3):185–212.
2. Wobst HJ, Mack KL, Brown DG, Brandon NJ, Shorter J. The clinical trial landscape in amyotrophic lateral sclerosis—Past, present, and future. Med Res Rev. 2020;40(4):1352–84.
3. Menon P, Vucic S. The Upper Motor Neuron—Improved knowledge from ALS and Related Clinical disorders. Brain Sci. 2021;11(8):958.
4. Menon P, Higashihara M, van den Bos M, Geevasinga N, Kiernan MC, Vucic S. Cortical hyperexcitability evolves with disease progression in ALS. Ann Clin Transl Neurol. 2020;7(5):733–41.
5. Menon P, Kiernan MC, Vucic S. Cortical hyperexcitability precedes lower motor neuron dysfunction in ALS. Clin Neurophysiol. 2015;126(4):803–9.
6. Eisen A, Braak H, Del Tredici K, Lemon R, Ludolph AC, Kiernan MC. Cortical influences drive amyotrophic lateral sclerosis. J Neurol Neurosurg Psychiatry. 2017;88(11):917–24.
7. Handley EE, Pitman KA, Dawkins E, Young KM, Clark RM, Jiang TC, et al. Synapse dysfunction of layer V pyramidal neurons precedes neurodegeneration in a mouse model of TDP-43 proteinopathies. Cereb Cortex. 2017;27(7):3630–47.
8. Birger A, Ottolenghi M, Perez L, Reubinoff B, Behar O. ALS-related human cortical and motor neurons survival is differentially affected by Sema3A. Cell Death Dis. 2018;9(3):1–9.
9. Brunet A, Stuart-Lopez G, Burg T, Scekic-Zahirovic J, Rouaux C. Cortical Circuit Dysfunction as a potential driver of amyotrophic lateral sclerosis. Front Neurosci. 2020;14:363.
10. Miller T, Cudkowicz M, Shaw PJ, Andersen PM, Atassi N, Bucelli RC, et al. Phase 1–2 trial of Antisense Oligonucleotide Tofersen for SOD1 ALS. N Engl J Med. 2020;383(2):109–19.
11. Terstappen GC, Meyer AH, Bell RD, Zhang W. Strategies for delivering therapeutics across the blood–brain barrier. Nat Rev Drug Discov. 2021;20(5):362–83.
12. Poulin-Brière A, Rezaei E, Pozzi S. Antibody-based therapeutic interventions for amyotrophic lateral sclerosis: a systematic literature review. Front Neurosci. 2021;15:790114.
13. Jablonski MR, Markandaiah SS, Jacob D, Meng NJ, Li K, Gennaro V, et al. Inhibiting drug efflux transporters improves efficacy of ALS therapeutics. Ann Clin Transl Neurol. 2014;1(12):996–1005.
14. Wu D, Chen Q, Chen X, Han F, Chen Z, Wang Y. The blood–brain barrier: structure, regulation, and drug delivery. Sig Transduct Target Ther. 2023;8(1):1–27.
15. Mirian A, Moszczynski A, Soleimani S, Aubert I, Zinman L, Abrahao A. Breached barriers: a scoping review of blood-central nervous System Barrier Pathology in Amyotrophic lateral sclerosis. Front Cell Neurosci. 2022;16:851563.
16. Pan Y, Nicolazzo JA. Altered blood-brain barrier and blood-spinal cord barrier dynamics in amyotrophic lateral sclerosis: impact on medication efficacy and safety. Br J Pharmacol. 2022;179(11):2577–88.
17. Steinruecke M, Lonergan RM, Selvaraj BT, Chandran S, Diaz-Castro B, Stavrou M. Blood-CNS barrier dysfunction in amyotrophic lateral sclerosis: proposed mechanisms and clinical implications. J Cereb Blood Flow Metab. 2023;43(5):642–54.
18. Schreiber S, Bernal J, Arndt P, Schreiber F, Müller P, Morton L, et al. Brain Vascular Health in ALS is mediated through Motor Cortex Microvascular Integrity. Cells. 2023;12(6):957.
19. Garbuzova-Davis S, Haller E, Saporta S, Kolomey I, Nicosia SV, Sanberg PR. Ultrastructure of blood-brain barrier and blood-spinal cord barrier in SOD1 mice modeling ALS. Brain Res. 2007;1157:126–37.
20. Zhong Z, Deane R, Ali Z, Parisi M, Shapovalov Y, O'Banion MK, et al. ALS-causing SOD1 mutants generate vascular changes prior to motor neuron degeneration. Nat Neurosci. 2008;11(4):420–2.
21. Cao MC, Cawston EE, Chen G, Brooks C, Douwes J, McLean D, et al. Serum biomarkers of neuroinflammation and blood-brain barrier leakage in amyotrophic lateral sclerosis. BMC Neurol. 2022;22(1):216.
22. Yoshikawa M, Aizawa S, Oppenheim RW, Milligan C. Neurovascular unit pathology is observed very early in disease progression in the mutant SOD1G93A mouse model of amyotrophic lateral sclerosis. Exp Neurol. 2022;353:114084.
23. Bataveljić D, Stamenković S, Bačić G, Andjus PR. Imaging cellular markers of neuroinflammation in the brain of the rat model of amyotrophic lateral sclerosis. Acta Physiol Hung. 2011;98(1):27–31.
24. Garbuzova-Davis S, Sanberg PR. Blood-CNS barrier impairment in ALS patients versus an animal model. Front Cell Neurosci. 2014;8:21.
25. Garbuzova-Davis S, Hernandez-Ontiveros DG, Rodrigues MCO, Haller E, Frisina-Deyo A, Mirtyl S, et al. Impaired blood-brain/spinal cord barrier in ALS patients. Brain Res. 2012;1469:114–28.
26. van Vliet EA, Iyer AM, Mesarosova L, Çolakoglu H, Anink JJ, van Tellingen O, et al. Expression and Cellular distribution of P-Glycoprotein and breast Cancer resistance protein in amyotrophic lateral sclerosis patients. J Neuropathol Exp Neurol. 2020;79(3):266–76.
27. Wasielewska JM, White AR. Focused Ultrasound-mediated drug delivery in humans - a path towards translation in neurodegenerative diseases. Pharm Res. 2022;39(3):427–39.
28. Ediriweera GR, Fletcher NL, Cowin G, Simpson JD, Chen L, Wasielewska JM et al. Enhancing the delivery of SOD1 antisense oligonucleotides to the murine brain using lipid nanoparticles and image-guided focused ultrasound. In Review; 2022 May.doi: https://doi.org/10.21203/rs.3.rs-1640138/v1
29. Shen Y, Zhang J, Xu Y, Sun S, Chen K, Chen S, et al. Ultrasound–enhanced brain delivery of edaravone provides additive amelioration on disease progression in an ALS mouse model. Brain Stimul. 2023;16(2):628–41.
30. Xia L, Hua L, Sun S, Yang X, Chen X, Chen S et al. Delivery of Arctiin via Ultrasound with Microbubbles Exerted Positive Effects on Motor Function in a Transgenic Mice Model of Amyotrophic Lateral Sclerosis. In: 2021 IEEE International Ultrasonics Symposium (IUS). 2021. pp. 1–4.
31. Abrahao A, Meng Y, Llinas M, Huang Y, Hamani C, Mainprize T, et al. First-in-human trial of blood–brain barrier opening in amyotrophic lateral sclerosis using MR-guided focused ultrasound. Nat Commun. 2019;10(1):4373.
32. Picher-Martel V, Valdmanis PN, Gould PV, Julien JP, Dupré N. From animal models to human disease: a genetic approach for personalized medicine in ALS. Acta Neuropathol Commun. 2016;4(1):70.
33. Oikari LE, Pandit R, Stewart R, Cuní-López C, Quek H, Sutharsan R, et al. Altered brain endothelial cell phenotype from a familial Alzheimer mutation and its potential implications for amyloid clearance and drug delivery. Stem Cell Rep. 2020;14(5):924–39.
34. Wasielewska JM, Szostak K, McInnes LE, Quek H, Chaves JCS, Liddell JR, et al. Patient-derived blood-brain barrier model for Screening Copper Bis(thiosemicarbazone) complexes as potential therapeutics in Alzheimer's Disease. ACS Chem Neurosci. 2024;15(7):1432–55.
35. Balez R, Berg T, Bax M, Muñoz SS, Cabral-da-Silva MC, Engel M, et al. The mRNA-based reprogramming of fibroblasts from a SOD1E101G familial amyotrophic lateral sclerosis patient to induced pluripotent stem cell line UOWi007. Stem Cell Res. 2020;42:101701.
36. Wasielewska JM, Chaves JCS, Johnston RL, Milton LA, Hernández D, Chen L, et al. A sporadic Alzheimer's blood-brain barrier model for developing ultrasound-mediated delivery of Aducanumab and anti-tau antibodies. Theranostics. 2022;12(16):6826–47.
37. Stebbins MJ, Wilson HK, Canfield SG, Qian T, Palecek SP, Shusta EV. Differentiation and characterization of human pluripotent stem cell-derived brain microvascular endothelial cells. Methods. 2016;101:93–102.
38. Chaves JCS, Wasielewska JM, Cuní-López C, Rantanen LM, Lee S, Koistinaho J et al. Alzheimer's disease brain endothelial-like cells reveal differential drug transporter expression and modulation by potentially therapeutic focused ultrasound. Neurotherapeutics. 2023;e00299.
39. Wasielewska JM, Bajracharya R, Johnston RL, Chaves JCS, Pébay A, Oikari LE, et al. Increased tau expression in the APOE4 blood-brain barrier model is associated with reduced anti-tau therapeutic antibody delivery in vitro. bioRxiv. 2023. https://doi.org/10.1101/2023.10.24.563706.

40. Lippmann ES, Al-Ahmad A, Azarin SM, Palecek SP, Shusta EV. A retinoic acid-enhanced, multicellular human blood-brain barrier model derived from stem cell sources. Sci Rep. 2014;4(1):4160.
41. Quek H, Cuní-López C, Stewart R, Colletti T, Notaro A, Nguyen TH, et al. ALS monocyte-derived microglia-like cells reveal cytoplasmic TDP-43 accumulation, DNA damage, and cell-specific impairment of phagocytosis associated with disease progression. J Neuroinflammation. 2022;19(1):58.
42. Ansbro MR, Shukla S, Ambudkar SV, Yuspa SH, Li L. Screening compounds with a Novel High-Throughput ABCB1-Mediated Efflux Assay identifies drugs with known therapeutic targets at risk for Multidrug Resistance Interference. PLoS ONE. 2013;8(4):e60334.
43. Pandit R, Leinenga G, Götz J. Repeated ultrasound treatment of tau transgenic mice clears neuronal tau by autophagy and improves behavioral functions. Theranostics. 2019;9(13):3754–67.
44. Swain N, Thakur M, Pathak J, Swain B. SOX2, OCT4 and NANOG: the core embryonic stem cell pluripotency regulators in oral carcinogenesis. J Oral Maxillofac Pathol. 2020;24(2):368–73.
45. Lippmann ES, Azarin SM, Kay JE, Nessler RA, Wilson HK, Al-Ahmad A, et al. Human blood-brain barrier endothelial cells derived from pluripotent stem cells. Nat Biotechnol. 2012;30(8):783–91.
46. Qosa H, Lichter J, Sarlo M, Markandaiah SS, McAvoy K, Richard JP, et al. Astrocytes drive upregulation of the multidrug resistance transporter ABCB1 (P-Glycoprotein) in endothelial cells of the blood-brain barrier in mutant superoxide dismutase 1-linked amyotrophic lateral sclerosis. Glia. 2016;64(8):1298–313.
47. Jablonski MR, Jacob DA, Campos C, Miller DS, Maragakis NJ, Pasinelli P, et al. Selective increase of two ABC drug efflux transporters at the blood-spinal cord barrier suggests induced pharmacoresistance in ALS. Neurobiol Dis. 2012;47(2):194–200.
48. Mohamed LA, Markandaiah S, Bonanno S, Pasinelli P, Trotti D. Excess glutamate secreted from astrocytes drives upregulation of P-glycoprotein in endothelial cells in amyotrophic lateral sclerosis. Exp Neurol. 2019;316:27–38.
49. Neumann M, Sampathu DM, Kwong LK, Truax AC, Micsenyi MC, Chou TT, et al. Ubiquitinated TDP-43 in frontotemporal lobar degeneration and amyotrophic lateral sclerosis. Science. 2006;314(5796):130–3.
50. Ling SC, Polymenidou M, Cleveland DW. Converging mechanisms in ALS and FTD: disrupted RNA and protein homeostasis. Neuron. 2013;79(3):416–38.
51. Ferrer I, Andrés-Benito P, Carmona M, Assialioui A, Povedano M. TDP-43 Vasculopathy in the spinal cord in sporadic amyotrophic lateral sclerosis (sALS) and Frontal Cortex in sALS/FTLD-TDP. J Neuropathol Exp Neurol. 2021;80(3):229–39.
52. Lipsman N, Meng Y, Bethune AJ, Huang Y, Lam B, Masellis M, et al. Blood-brain barrier opening in Alzheimer's disease using MR-guided focused ultrasound. Nat Commun. 2018;9(1):2336.
53. Qian TC, Maguire S, Canfield SG, Bao X, Olson W, Shusta E et al. Directed differentiation of human pluripotent stem cells to blood-brain barrier endothelial cells. Sci Adv. 2017;3(11).
54. Lu TM, Houghton S, Magdeldin T, Durán JGB, Minotti AP, Snead A et al. Pluripotent stem cell-derived epithelium misidentified as brain microvascular endothelium requires ETS factors to acquire vascular fate. Proc Natl Acad Sci U S A. 2021;118(8).
55. Srinivasan B, Kolli AR, Esch MB, Abaci HE, Shuler ML, Hickman JJ. TEER measurement techniques for in vitro barrier model systems. J Lab Autom. 2015;20(2):107–26.
56. Katt ME, Mayo LN, Ellis SE, Mahairaki V, Rothstein JD, Cheng L, et al. The role of mutations associated with familial neurodegenerative disorders on blood–brain barrier function in an iPSC model. Fluids Barriers CNS. 2019;16(1):20.
57. Gasca-Salas C, Fernández-Rodríguez B, Pineda-Pardo JA, Rodríguez-Rojas R, Obeso I, Hernández-Fernández F, et al. Blood-brain barrier opening with focused ultrasound in Parkinson's disease dementia. Nat Commun. 2021;12(1):779.
58. Chen L, Sutharsan R, Lee JL, Cruz E, Asnicar B, Palliyaguru T, et al. Claudin-5 binder enhances focused ultrasound-mediated opening in an in vitro blood-brain barrier model. Theranostics. 2022;12(5):1952–70.
59. Sheikov N, Mcdannold N, Sharma S, Hynynen K. Effect of focused Ultrasound Applied with an ultrasound contrast Agent on the tight Junctional Integrity of the Brain Microvascular Endothelium. Ultrasound Med Biol. 2008;34(7):1093–104.
60. Kline-Schoder AR, Chintamen S, Willner MJ, DiBenedetto MR, Noel RL, Batts AJ et al. Characterization of the responses of brain macrophages to focused ultrasound-mediated blood–brain barrier opening. Nat Biomed Eng. 2023;1–14.
61. Leinenga G, Goetz J. Scanning ultrasound removes amyloid-beta and restores memory in an Alzheimer's disease mouse model. Sci Transl Med. 2015;7(278):278ra33.
62. Ji R, Karakatsani ME, Burgess M, Smith M, Murillo MF, Konofagou EE. Cavitation-modulated inflammatory response following focused ultrasound blood-brain barrier opening. J Control Release. 2021;337:458–71.
63. Kovacs ZI, Kim S, Jikaria N, Qureshi F, Milo B, Lewis BK, et al. Disrupting the blood-brain barrier by focused ultrasound induces sterile inflammation. Proc Natl Acad Sci U S A. 2017;114(1):E75–84.
64. McMahon D, Bendayan R, Hynynen K. Acute effects of focused ultrasound-induced increases in blood-brain barrier permeability on rat microvascular transcriptome. Sci Rep. 2017;7(1):45657.
65. Smyth LCD, Rustenhoven J, Park TIH, Schweder P, Jansson D, Heppner PA, et al. Unique and shared inflammatory profiles of human brain endothelia and pericytes. J Neuroinflammation. 2018;15(1):138.
66. Al-Soudi A, Kaaij MH, Tas SW. Endothelial cells: from innocent bystanders to active participants in immune responses. Autoimmun Rev. 2017;16(9):951–62.
67. Evans MC, Couch Y, Sibson N, Turner MR. Inflammation and neurovascular changes in amyotrophic lateral sclerosis. Mol Cell Neurosci. 2013;53:34–41.
68. de Luna N, Carbayo Á, Dols-Icardo O, Turon-Sans J, Reyes-Leiva D, Illan-Gala I et al. Neuroinflammation-related proteins NOD2 and Spp1 are abnormally upregulated in amyotrophic lateral sclerosis. Neurol Neuroimmunol Neuroinflamm. 2023;10(2).
69. Nisbet RM, Van Der Jeugd A, Leinenga G, Evans HT, Janowicz PW, Götz J. Combined effects of scanning ultrasound and a tau-specific single chain antibody in a tau transgenic mouse model. Brain. 2017;140(5):1220–30.
70. Janowicz PW, Leinenga G, Götz J, Nisbet RM. Ultrasound-mediated blood-brain barrier opening enhances delivery of therapeutically relevant formats of a tau-specific antibody. Sci Rep. 2019;9(1):9255–9255.
71. Bajracharya R, Cruz E, Götz J, Nisbet RM. Ultrasound-mediated delivery of novel tau-specific monoclonal antibody enhances brain uptake but not therapeutic efficacy. J Control Release. 2022;349:634–48.
72. Dharmadasa T, Kiernan MC. Riluzole, disease stage and survival in ALS. Lancet Neurol. 2018;17(5):385–6.
73. Shefner J, Heiman-Patterson T, Pioro EP, Wiedau-Pazos M, Liu S, Zhang J, et al. Long-term edaravone efficacy in amyotrophic lateral sclerosis: post-hoc analyses of study 19 (MCI186-19). Muscle Nerve. 2020;61(2):218–21.
74. Miller TM, Cudkowicz ME, Genge A, Shaw PJ, Sobue G, Bucelli RC, et al. Trial of Antisense Oligonucleotide Tofersen for SOD1 ALS. N Engl J Med. 2022;387(12):1099–110.
75. Milane A, Fernandez C, Vautier S, Bensimon G, Meininger V, Farinotti R. Minocycline and riluzole brain disposition: interactions with p-glycoprotein at the blood-brain barrier. J Neurochem. 2007;103(1):164–73.
76. Milane A, Vautier S, Chacun H, Meininger V, Bensimon G, Farinotti R, et al. Interactions between riluzole and ABCG2/BCRP transporter. Neurosci Lett. 2009;452(1):12–6.
77. Milane A, Fernandez C, Dupuis L, Buyse M, Loeffler JP, Farinotti R, et al. P-glycoprotein expression and function are increased in an animal model of amyotrophic lateral sclerosis. Neurosci Lett. 2010;472(3):166–70.
78. Bauer HC, Krizbai IA, Bauer H, Traweger A. You shall not pass—tight junctions of the blood brain barrier. Front Neurosci. 2014;8:392.
79. Ohshima M, Kamei S, Fushimi H, Mima S, Yamada T, Yamamoto T. Prediction of drug permeability using in Vitro blood–brain barrier models with Human Induced Pluripotent Stem cell-derived brain microvascular endothelial cells. Biores Open Access. 2019;8(1):200–9.
80. Roux GL, Jarray R, Guyot AC, Pavoni S, Costa N, Théodoro F, et al. Proof-of-Concept Study of Drug Brain Permeability between in vivo human brain and an in Vitro iPSCs-Human blood-brain barrier model. Sci Rep. 2019;9:16310.
81. Prell T, Vlad B, Gaur N, Stubendorff B, Grosskreutz J. Blood–brain barrier disruption is not Associated with Disease aggressiveness in amyotrophic lateral sclerosis. Front Neurosci. 2021;15.
82. Meucci G, Rossi G, Bettini R, Montanaro D, Gironelli L, Voci L, et al. Laser nephelometric evaluation of albumin, IgG and alpha 2-macroglobulin: applications to the study of alterations of the blood-brain barrier. J Neurol Sci. 1993;118(1):73–8.
83. Wu Y, Yang X, Li X, Wang H, Wang T. Elevated cerebrospinal fluid homocysteine is associated with blood-brain barrier disruption in amyotrophic lateral sclerosis patients. Neurol Sci. 2020;41(7):1865–72.
84. Verde F, Ferrari I, Maranzano A, Ciusani E, Torre S, Milone I, et al. Relationship between cerebrospinal fluid/serum albumin quotient and phenotype in amyotrophic lateral sclerosis: a retrospective study on 328 patients. Neurol Sci. 2023;44(5):1679–85.

85. Gavard J. Endothelial permeability and VE-cadherin. Cell Adh Migr. 2014;8(2):158–64.
86. Tziortzouda P, Van Den Bosch L, Hirth F. Triad of TDP43 control in neurodegeneration: autoregulation, localization and aggregation. Nat Rev Neurosci. 2021;22(4):197–208.
87. Oiwa K, Watanabe S, Onodera K, Iguchi Y, Kinoshita Y, Komine O, et al. Monomerization of TDP-43 is a key determinant for inducing TDP-43 pathology in amyotrophic lateral sclerosis. Sci Adv. 2023;9(31):eadf6895.
88. Rubio MA, Herrando-Grabulosa M, Velasco R, Blasco I, Povedano M, Navarro X. TDP-43 cytoplasmic translocation in the skin fibroblasts of ALS patients. Cells. 2022;11(2):209.
89. Sabatelli M, Zollino M, Conte A, Del Grande A, Marangi G, Lucchini M, et al. Primary fibroblasts cultures reveal TDP-43 abnormalities in amyotrophic lateral sclerosis patients with and without SOD1 mutations. Neurobiol Aging. 2015;36(5):e20055–200513.
90. Ratti A, Gumina V, Lenzi P, Bossolasco P, Fulceri F, Volpe C, et al. Chronic stress induces formation of stress granules and pathological TDP-43 aggregates in human ALS fibroblasts and iPSC-motoneurons. Neurobiol Dis. 2020;145:105051.
91. Garbuzova-Davis S, Thomson A, Kurien C, Shytle RD, Sanberg PR. Potential new complication in drug therapy development for amyotrophic lateral sclerosis. Expert Rev Neurother. 2016;16(12):1397–405.
92. Kovacs ZI, Burks SR, Frank JA. Focused ultrasound with microbubbles induces sterile inflammatory response proportional to the blood brain barrier opening: attention to experimental conditions. Theranostics. 2018;8(8):2245–8.
93. Pardridge WM. The blood-brain barrier: Bottleneck in Brain Drug Development. NeuroRX. 2005;2(1):3–14.
94. Riemenschneider H, Simonetti F, Sheth U, Katona E, Roth S, Hutten S, et al. Targeting the glycine-rich domain of TDP-43 with antibodies prevents its aggregation in vitro and reduces neurofilament levels in vivo. Acta Neuropathol Commun. 2023;11(1):112.
95. Pozzi S, Thammisetty SS, Codron P, Rahimian R, Plourde KV, Soucy G, et al. Virus-mediated delivery of antibody targeting TAR DNA-binding protein-43 mitigates associated neuropathology. J Clin Invest. 2019;129(4):1581–95.
96. Pozzi S, Codron P, Soucy G, Renaud L, Cordeau PJ, Dutta K et al. Monoclonal full-length antibody against TAR DNA binding protein 43 reduces related proteinopathy in neurons. JCI Insight. 2020;5(21).
97. Afroz T, Chevalier E, Audrain M, Dumayne C, Ziehm T, Moser R, et al. Immunotherapy targeting the C-terminal domain of TDP-43 decreases neuropathology and confers neuroprotection in mouse models of ALS/FTD. Neurobiol Dis. 2023;179:106050.
98. Sevigny J, Chiao P, Bussière T, Weinreb PH, Williams L, Maier M, et al. The antibody aducanumab reduces Aβ plaques in Alzheimer's disease. Nature. 2016;537(7618):50–6.
99. Schneider L. A resurrection of aducanumab for Alzheimer's disease. Lancet Neurol. 2020;19(2):111–2.
100. van Dyck CH, Swanson CJ, Aisen P, Bateman RJ, Chen C, Gee M, et al. Lecanemab in Early Alzheimer's Disease. N Engl J Med. 2023;388(1):9–21.
101. Sims JR, Zimmer JA, Evans CD, Lu M, Ardayfio P, Sparks J, et al. Donanemab in early symptomatic Alzheimer Disease: the TRAILBLAZER-ALZ 2 Randomized Clinical Trial. JAMA. 2023;330(6):512–27.
102. Rezai AR, D'Haese PF, Finomore V, Carpenter J, Ranjan M, Wilhelmsen K, et al. Ultrasound blood–brain barrier opening and Aducanumab in Alzheimer's Disease. N Engl J Med. 2024;390(1):55–62.
103. Li Y, Balasubramanian U, Cohen D, Zhang PW, Mosmiller E, Sattler R, et al. A Comprehensive Library of Familial Human Amyotrophic lateral sclerosis Induced Pluripotent Stem cells. PLoS ONE. 2015;10(3):e0118266.
104. Annika Armulik G, Genové M, Mäe MH, Nisancioglu E, Wallgard C, Niaudet, et al. Pericytes regulate the blood–brain barrier. Nature. 2010;468(7323):557–61.
105. Bell RD, Winkler EA, Sagare AP, Singh I, Larue B, Deane R, et al. Pericytes Control Key Neurovascular Functions and neuronal phenotype in the adult brain and during Brain Aging. Neuron. 2010;68(3):409–27.
106. Heithoff BP, George KK, Phares AN, Zuidhoek IA, Munoz-Ballester C, Robel S. Astrocytes are necessary for blood–brain barrier maintenance in the adult mouse brain. Glia. 2021;69(2):436–72.
107. Manu DR, Slevin M, Barcutean L, Forro T, Boghitoiu T, Balasa R. Astrocyte involvement in blood–brain barrier function: a critical update highlighting Novel, Complex, neurovascular interactions. Int J Mol Sci. 2023;24(24):17146.
108. Paranjape AN, D'Aiuto L, Zheng W, Chen X, Villanueva FS. A multicellular brain spheroid model for studying the mechanisms and bioeffects of ultrasound-enhanced drug penetration beyond the blood–brain barrier. Sci Rep. 2024;14(1):1909.
109. Ge S, Pachter JS. Isolation and culture of microvascular endothelial cells from murine spinal cord. J Neuroimmunol. 2006;177(1–2):209–14.
110. Henkel JS, Beers DR, Wen S, Bowser R, Appel SH. Decreased mRNA expression of tight junction proteins in lumbar spinal cords of patients with ALS. Neurology. 2009;72(18):1614–6.
111. Garbuzova-Davis S, Woods RL, Louis MK, Zesiewicz TA, Kuzmin-Nichols N, Sullivan KL, et al. Reduction of circulating endothelial cells in peripheral blood of ALS patients. PLoS ONE. 2010;5(5):e10614.
112. Kung Y, Chen KY, Liao WH, Hsu YH, Wu CH, Hsiao MY, et al. Facilitating drug delivery in the central nervous system by opening the blood-cerebrospinal fluid barrier with a single low energy shockwave pulse. Fluids Barriers CNS. 2022;19(1):3.
113. Smith P, Ogrodnik N, Satkunarajah J, O'Reilly MA. Characterization of ultrasound-mediated delivery of trastuzumab to normal and pathologic spinal cord tissue. Sci Rep. 2021;11(1):4412.
114. Payne A, Hawryluk G, Anzai Y, Odéen H, Ostlie M, Reichert E et al. Magnetic resonance imaging-guided focused ultrasound to increase localized blood-spinal cord barrier permeability. Neural Regen Res. 2017;12.

Publisher's Note